



HAL
open science

Which minerals control the Nd–Hf–Sr–Pb isotopic compositions of river sediments?

Marion Garçon, Catherine Chauvel, Christian France-Lanord, Mara Limonta,
Eduardo Garzanti

► To cite this version:

Marion Garçon, Catherine Chauvel, Christian France-Lanord, Mara Limonta, Eduardo Garzanti. Which minerals control the Nd–Hf–Sr–Pb isotopic compositions of river sediments?. *Chemical Geology*, 2014, 364, pp.42 - 55. 10.1016/j.chemgeo.2013.11.018 . hal-01769091

HAL Id: hal-01769091

<https://hal.univ-lorraine.fr/hal-01769091v1>

Submitted on 23 Aug 2022

HAL is a multi-disciplinary open access archive for the deposit and dissemination of scientific research documents, whether they are published or not. The documents may come from teaching and research institutions in France or abroad, or from public or private research centers.

L'archive ouverte pluridisciplinaire **HAL**, est destinée au dépôt et à la diffusion de documents scientifiques de niveau recherche, publiés ou non, émanant des établissements d'enseignement et de recherche français ou étrangers, des laboratoires publics ou privés.



Distributed under a Creative Commons Attribution - NonCommercial - NoDerivatives 4.0 International License

1
2
3
4
5
6
7
8
9
10
11
12
13
14
15
16
17
18
19
20
21
22
23
24
25
26

Which minerals control the Nd-Hf-Sr-Pb isotopic compositions of river sediments?

Marion Garçon^{1*}, Catherine Chauvel¹, Christian France-Lanord², Mara Limonta³,
Eduardo Garzanti³

¹ ISTerre, CNRS, Université Joseph Fourier de Grenoble, BP 53, 38041 Grenoble Cedex 09, France

² CRPG-CNRS, 15, rue Notre Dame des Pauvres, 54501 Vandoeuvre-lès-Nancy, France

³ Laboratorio di Petrografia del Sedimentario, Dipartimento di Scienze Geologiche e Geotecnologie, Università di Milano-Bicocca, 20126 Milano, Italy

* Corresponding author

Present address: Carnegie Institution of Washington, Department of Terrestrial Magnetism, 5241 Broad Branch Road, NW, Washington D.C., 20015, United States

e-mail: garconm@dtm.ciw.edu

Tel: +1 202 478 8477

27 **Abstract**

28 River sediments naturally sample and average large areas of eroded continental
29 crust. They are ideal targets not only for provenance studies based on isotopic
30 compositions, but also can be used to establish average continental crust isotopic values.
31 In large fluvial systems, however, mineral sorting processes significantly modify the
32 mineralogy, and thus the geochemistry of the transported sediments. We still do not
33 know, in any quantitative way, to what extent mineral sorting affects and fractionates the
34 isotopic compositions of river sediments. Here, we focus on this issue and try to decipher
35 the role of each mineral species in the bulk isotopic compositions of bedloads and
36 suspended loads sampled at the outflow of the Ganga River that drains the Himalayan
37 mountain range.

38 We analyzed Nd, Hf, Sr, and Pb isotopic compositions as well as trace element
39 contents of a large number of pure mineral fractions (K-feldspar, plagioclase, muscovite,
40 biotite, magnetite, zircon, titanite, apatite, monazite/allanite, amphibole, epidote, garnet,
41 carbonate and clay) separated from bedload and bank sediments. We combine these data
42 with mineral proportions typical of the Ganga sediments to perform Monte-Carlo
43 simulations that quantify the contributions of individual mineral species to the Nd, Hf, Sr,
44 and Pb isotopic budgets of bedloads and suspended loads.

45 We show that the isotopic systematics of river sediments are buffered by very few
46 minerals. Despite their extremely low proportions in sediments, zircon and
47 monazite/allanite control Hf and Nd isotopes, respectively. Feldspars, epidote, and
48 carbonate buffer the Sr isotopic budget while clay, feldspars, and heavy minerals
49 dominate Pb isotopes. Hafnium, Sr, and Pb isotopic differences between bedloads and
50 suspended loads are well explained by their different mineral compositions. This

51 confirms that Hf, Sr and Pb isotopic compositions of sediments are strongly biased by
52 mineral sorting processes during fluvial transport; hence they do not always constitute
53 good proxies for provenance studies. In addition, we anticipate that fractionation of the
54 isotopic systems continues at the river/ocean interface to deliver sediments to the deep
55 ocean that are not necessarily similar to their crustal precursors, creating a systematic
56 bias between the compositions of crustal sources and oceanic sediments.

57

58 **Keywords:** isotopic fractionation, bedload, suspended load, continental crust,
59 Himalayas, minerals

60

61

62

63

64

65

66

67

68

69

70

71

72

73 **1. Introduction**

74 Because they integrate large portions of continental crust exposed to weathering,
75 river sediments from worldwide fluvial systems have been widely used to trace sediment
76 provenance, estimate the average isotopic composition of the upper continental crust, and
77 constrain its evolution through time (Goldstein et al., 1984; Goldstein and Jacobsen, 1988;
78 Asmerom and Jacobsen, 1993; Allègre et al., 1996; Clift et al., 2002; Singh and France-
79 Lanord, 2002; Millot et al., 2004; Kamber et al., 2005; Richards et al., 2005; Roddaz et al.,
80 2005; Singh et al., 2008; Cina et al., 2009; Belousova et al., 2010; Hawkesworth et al., 2010;
81 Wu et al., 2010; Dhuime et al., 2011; Padoan et al., 2011). Most studies assume that the
82 isotopic compositions of river sediments reflect that of the drained continental area.
83 However, depending on its size, shape, and density, detrital material transported by rivers
84 is segregated within the water column by hydrodynamic processes: fast-settling coarse
85 and heavy minerals concentrate in bedloads while fine, platy and light minerals are
86 preferentially transported in suspension, and at different depths in the water column
87 depending on their settling velocities (Singh and France-Lanord, 2002; Komar, 2007; Galy
88 et al., 2008; Garzanti et al., 2008). Because chemical elements are carried in different
89 amounts by the various minerals, it is now well described that mineral sorting processes
90 lead to large chemical variability between bedload and suspended load sediments
91 (Garzanti et al., 2010; Bouchez et al., 2011; Garzanti et al., 2011; Lupker et al., 2011; 2012).
92 In contrast, our knowledge of how such processes affect the Nd, Hf, Sr and Pb isotopic
93 compositions of sediments is relatively limited. While several studies have pointed out
94 Nd, Hf, Sr and Pb isotopic fractionations between fine and coarse-grained sediments due
95 to mineral sorting processes (Patchett et al., 1984; McLennan et al., 1989; Revel et al.,
96 1996; Eisenhauer et al., 1999; Singh and France-Lanord, 2002; Chauvel et al., 2008; Bayon

97 et al., 2009; Carpentier et al., 2009; Chauvel et al., 2009; Vervoort et al., 2011; Garçon et
98 al., 2013a, 2013b), the influence of each mineral species on the isotopic composition of
99 sediments has never been thoroughly quantified.

100 In this paper, we report trace element contents and Nd, Hf, Sr and Pb isotopic
101 compositions for a large number of pure mineral fractions separated from a bedload and
102 a bank sediment sampled at the outflow of the Ganga fluvial system in the Bangladesh
103 delta. Using Monte-Carlo simulations, we combine these data with mineral proportions
104 reported by Garzanti et al. (2010; 2011) and Lupker et al. (2012) in river sediments
105 sampled at the same location to (1) evaluate the individual contribution of each mineral
106 species to the Nd, Hf, Sr and Pb isotopic budgets of bedloads and suspended loads and (2)
107 determine if the known mineralogy of bedloads and suspended loads accounts for the
108 observed difference in isotopic compositions. Finally, we discuss the implications of our
109 results for sediment provenance studies based on isotope data and for large-scale isotopic
110 partitioning between continental and oceanic sediments.

111 **2. Studied Area and Samples**

112 The studied mineral fractions were separated from two samples (bank sediment
113 BGP 6 and bedload BR 717) collected at the outflow of the Ganga River, before the
114 confluence with the Brahmaputra River (Figure 1). The sampling site was selected
115 because it is located downstream, far away from the mountain range. As a consequence,
116 the sediments integrate all materials transported by the Ganga River and its tributaries.
117 These rivers belong to one of the largest fluvial systems on Earth (Milliman and Meade,
118 1983), stretch over more than 2500 km and deliver about four hundred million tons of
119 sediments to the ocean each year (Lupker et al., 2011). Such sediments are dominantly
120 (>95%) derived from the Himalayan mountain range with minor contributions from the

121 Deccan Trapps and Indian craton supplied by the southern tributaries of the Ganga (Galy
122 and France-Lanord, 2001; Singh et al., 2008; Lupker et al., 2011). Himalayan materials
123 mainly consist of sedimentary series and crystalline metamorphic rocks (e.g., Le Fort,
124 1975). Because of the large lithological and chemical diversity of Himalayan rocks, the
125 Ganga basin can be considered as a representative portion of the upper continental crust.
126 All minerals analyzed in our study are thus ubiquitous in the erosion products of any
127 upper continental crust exposed to weathering (McLennan, 1989; Taylor and McLennan,
128 1995; McLennan, 2001) and our results should be relevant for river sediments sampled
129 in other worldwide fluvial systems draining large continental areas.

130 The second major advantage of the selected site is that these sediments were
131 extensively studied for their mineralogy by Garzanti et al. (2010; 2011) and Lupker et al.
132 (2012) (Supplementary Table 1). These authors showed that bedloads and suspended
133 loads share quite similar types of minerals but in different proportions. Surface
134 suspended loads are generally finer and relatively rich in micas and clays while bedloads
135 tend to be coarser and richer in quartz and heavy minerals. Among the heavy minerals
136 that are commonly found in the Ganga sediments, amphibole, epidote and garnet are the
137 most abundant but many others are also present: titanite, zircon, rutile, apatite, monazite,
138 tourmaline and allanite for example (Garzanti et al., 2010; 2011). Detailed mineral
139 proportions in the Ganga bedloads and suspended loads are listed in Supplementary
140 Table 1.

141 Finally, several studies have reported major and trace element contents, as well as
142 Nd, Hf, and Pb isotopic compositions, of bulk suspended loads and bedloads from this
143 sampling site (Galy and France-Lanord, 2001; Lupker et al., 2011; 2012; Garçon et al.
144 2012, 2013a; 2013b; see Supplementary Table 2). We used these data to evaluate the role
145 of individual minerals in the bulk isotopic budget of river sediments. Because no Sr

146 isotopic data exist in the literature for unleached bedloads and suspended loads, we
147 analyzed the bulk Sr isotopic compositions of two bedloads (BR 717 and BR 418), one
148 bank sediment (BGP 6) and 2 suspended loads (BR 414 and BR 412) sampled in the
149 Bangladesh delta (Figure 1). The trace element data and the Nd, Hf, and Pb isotopic
150 compositions of these five samples are reported in Supplementary Table 2. The detailed
151 sampling methods and the major element data can be found in Galy and France-Lanord
152 (2001), Lupker et al. (2011; 2012) and Garçon et al. (2013a; 2013b). We also analyzed the
153 Sr isotopic compositions of several grain-size fractions separated from a suspended load
154 from the Ganga River (sample BR 522, Figure 1) to help us interpreting the Sr results of
155 the Monte-Carlo simulations.

156 **3. Methods**

157 **3.1. Mineral separation**

158 The starting material consists of several kilos of sediment collected during the
159 monsoon season. With the exception of the clay fraction separated from bank sediment
160 BGP 6, all mineral fractions were separated from bedload BR 717 dredged in the main
161 channel of the Ganga River. This sample was first washed and dried, then divided into 3
162 grain-size fractions by sieving: 63-100 μm , 125-250 μm , and >250 μm . For each fraction,
163 we used successive centrifugations in heavy liquids (sodium metatungstate and
164 methylene iodide) to separate minerals and partial freezing in liquid nitrogen to recover
165 them. After this step, some of the minerals were isolated using a hand magnet or the
166 Frantz isodynamic magnetic separator. Biotite, muscovite, plagioclase, quartz, and K-
167 feldspar were isolated from the >250 μm fraction; magnetite, amphibole, apatite, garnet,
168 epidote, titanite, monazite, allanite, and zircon from the 63-100 μm and/or the 125-250

169 μm fractions. Each mineral fraction was finally carefully purified under the binocular and
170 polarizing microscopes to remove impurities.

171 Because monazite and allanite were very small and difficult to distinguish from
172 each other, we analyzed an impure fraction containing high amounts of both minerals. In
173 the rest of the paper, this fraction is called the “monazite/allanite fraction”. Similarly, we
174 could not remove all impurities in the apatite fraction; hence we analyzed an impure
175 fraction highly enriched in apatite. Following Galy et al. (1999), the composition of the
176 carbonate fraction was obtained using a 1N acetic acid leaching procedure for one hour
177 in an ultrasonic bath. To ensure a pure carbonate fraction and avoid dissolution of other
178 minerals or contamination by clay minerals, we leached a coarse fraction containing only
179 carbonate, quartz, K-feldspar, plagioclase, and few phyllosilicates (non-magnetic 125-250
180 μm fraction with a density $< 2.90 \text{ g.cm}^{-3}$). The carbonate-rich leachate was then isolated
181 by centrifugation and evaporated on a hot plate. Finally, a clay fraction, selected as the < 2
182 μm fraction, was separated by sieving and settling from bank sediment BGP 6 because we
183 lacked sufficient material to recover it from bedload BR 717.

184 For each mineral species, only one fraction was separated and analyzed; the only
185 exception is the K-feldspar fraction (Table 1). We recognized that multiple analyzes of the
186 same mineral species could have been interesting to assess the compositional
187 heterogeneity of the Himalayan minerals. However, due to the limited quantity of starting
188 material and the time-consuming work involved in the handpicking procedure we could
189 not perform other duplicate analyses. We are however confident that the measured
190 fractions should be representative of the mineral populations because for each mineral
191 separate, the number of grains present in the analyzed fraction was always higher than a
192 thousand. For example, the 5mg fraction of zircons analyzed in this study most probably
193 contains between 1,000 to 2,000 zircon grains assuming that grains are spherical with a

194 mean diameter of 50-60 μm , as suggested by Garzanti et al. (2010; 2011) and Garçon et
195 al. (2013b).

196

197 **3.2. Chemistry**

198 For each mineral separate, we performed a single dissolution used to analyze both
199 trace element concentrations and Nd, Hf and Sr isotopes. Note that Pb isotopic
200 compositions of these sediments were previously published by Garçon et al. (2013b).
201 Methods used to obtain Pb data are described in this latter paper.

202 After washing with ultrapure water, 5 to 100 mg of mineral grains or powder were
203 first attacked for 2 days in 14N HNO_3 on a hot plate at 130°C, then evaporated and
204 dissolved in a mixture of HF and HClO_4 in teflon containers placed in steel PARR bombs
205 for 10 days at 200°C to ensure complete dissolution. For bulk bedloads and suspended
206 loads, 50 to 100 mg of fine powder were dissolved using the same procedure as for the
207 mineral fractions. Finally, the bulk suspended load BR 522 and its grain-size fractions,
208 separated using settling and sieving techniques, were leached in 1N acetic acid for one
209 hour in an ultrasonic bath to remove the carbonates before being digested following the
210 same dissolution procedure as the one described above.

211 We measured trace element concentrations by ICP-MS with a dilution factor of
212 5000 and the equivalent of 2mg of sample. Measurements were performed using an
213 Agilent 7500ce ICP-MS in Grenoble (France). Oxide interference and analytical drift were
214 corrected following the procedure of Chauvel et al. (2011). BR-24 rock standards were
215 measured every four samples to calibrate and convert peak signals into concentrations
216 offline. To ensure the validity of our results, international rock standards were run as

217 unknown samples, including sedimentary materials such as JSd-2 (see Supplementary
218 Table 3).

219 Hafnium, Nd and Sr were isolated from the same aliquot using the ion resin
220 techniques and following the procedure described by Chauvel et al. (2011). Hafnium was
221 recovered in three steps using a first column filled with cationic resin (AG50W-X8) to
222 isolate the High Field Strength Elements (HFSE) followed by a second anion resin column
223 (AG1-X8) and a third cation resin column (AG50W-X8) to isolate Hf from the other HFSE.
224 Nd was recovered in two steps: a first cation resin column (AG50W-X8) to isolate the Rare
225 Earth Elements (REE) and a second column filled with Ln-Spec resin to separate Nd from
226 the other REE. Finally, Sr was isolated using two successive columns filled with cationic
227 resin (AG50W-X8) and Sr-Spec resin. Total procedural blanks were < 80 pg for Nd (n=1),
228 < 35 pg for Hf (n=2) and < 140 pg for Sr (n=2). These small amounts can be considered
229 negligible compared to the amount of Nd, Hf and Sr isolated in all samples. Nd and Hf
230 isotopes were measured on a Nu Plasma MC-ICP-MS at the ENS Lyon (France). Nd isotopic
231 compositions were normalized to $^{146}\text{Nd}/^{144}\text{Nd}=0.7219$ and Hf isotopic compositions to
232 $^{179}\text{Hf}/^{177}\text{Hf}=0.7325$. The Ames-Rennes Nd and Ames-Grenoble Hf reference standards run
233 every two or three samples yielded average $^{143}\text{Nd}/^{144}\text{Nd} = 0.511953 \pm 8$ (2σ , $n = 15$) and
234 $^{176}\text{Hf}/^{177}\text{Hf} = 0.282157 \pm 18$ (2σ , $n = 14$), respectively. We used the recommended values
235 published by Chauvel and Blichert-Toft (2001) and Chauvel et al. (2011) for these two
236 standards to correct the analytical drift all through the measurement sequence. Sr
237 isotopic compositions were measured using a solid source ThermoScientific Triton mass
238 spectrometer in Brest (France) and normalized to $^{86}\text{Sr}/^{88}\text{Sr}=0.1194$. The NBS 987
239 reference material yielded average $^{87}\text{Sr}/^{86}\text{Sr} = 0.710270 \pm 7$ (2σ , $n = 10$) and values
240 measured for the samples were not normalized.

241 **4. Results**

242 **4.1. Trace element concentrations**

243 Trace element concentrations measured in the mineral fractions are reported in Table 1
244 and shown in Figure 2 as spidergrams normalized to the average composition of upper
245 continental crust (Rudnick and Gao, 2003). Except for mobile elements such as Cs, Rb, Ba,
246 Sr, Li, Co, or Ni, heavy minerals (Figure 2a) generally display higher trace element
247 contents than light minerals (Figure 2b). The trace element patterns of the various
248 minerals are generally consistent with published values (e.g., Götze and Lewis, 1994; Bea,
249 1996; Garçon et al., 2011; Garzanti et al., 2011). Zircon and garnet show typical depletions
250 in light REE while monazite/allanite show depletion in heavy REE. The REE distributions
251 of other minerals, including light minerals, are rather flat. The monazite/allanite and
252 zircon separates clearly exhibit the highest concentrations in LREE (including Nd) and Hf,
253 respectively, with enrichment factors > 1000 (see Figure 2). The highest Pb contents are
254 found in clay (95 ppm) and K-feldspar (75 ppm). The highest Sr concentrations are found
255 in epidote (1509 ppm), carbonate (526 ppm), K-feldspar (243 ppm) and plagioclase (195
256 ppm). Both apatite and monazite/allanite fractions display lower REE and higher Zr, Hf
257 concentrations compared to what could be expected in pure apatite and
258 monazite/allanite separates (Ayres and Harris, 1997; Garçon et al., 2011; Garzanti et al.,
259 2011), a feature probably due to the presence of impurities such as light minerals and
260 zircon grains. This can easily be explained by the fact that we were unable to purify the
261 apatite and monazite/allanite fractions under the binocular microscope due to the very
262 small size of the minerals. Similarly, the quartz fraction contains anomalously high REE
263 and Sr concentrations compared to what is usually obtained in pure quartz (see for

264 example Monecke et al., 2000 and Garzanti et al., 2010). It is thus likely that this fraction
265 also contains impurities.

266

267 **4.2. Isotopic compositions**

268 The Nd, Hf and Sr isotopic compositions for all mineral separates are reported in
269 Table 1. No Hf isotopic composition could be measured for the carbonate fraction because
270 of its very low Hf concentration. We also did not measure the isotopic compositions of the
271 quartz fraction and the Hf and Sr isotopes of the monazite/allanite-rich and the apatite-
272 rich separate because of the presence of other minerals in these separates that could
273 strongly influence the measured isotopic compositions.

274 Nd, Hf and Sr isotopic compositions span large ranges of values between 0.511732
275 and 0.512235 for $^{143}\text{Nd}/^{144}\text{Nd}$, 0.281970 and 0.282803 for $^{176}\text{Hf}/^{177}\text{Hf}$ and 0.7125 and
276 0.8313 for $^{87}\text{Sr}/^{86}\text{Sr}$. The monazite/allanite fraction has the least radiogenic Nd isotopic
277 compositions of all minerals while the zircon separate has the least radiogenic Hf isotopic
278 compositions. Biotite and muscovite, known for their very high Rb/Sr ratios, have
279 accordingly highly radiogenic Sr isotopic compositions (0.8123 and 0.8313, respectively).
280 By contrast, epidote and carbonate have the least radiogenic Sr isotopic compositions
281 (0.7125 and 0.7139) of all minerals.

282 Sr isotopic compositions measured in bulk bedloads, banks and suspended loads
283 from the Ganga River are listed in Table 2. They are particularly radiogenic with $^{87}\text{Sr}/^{86}\text{Sr}$
284 varying between 0.7546 and 0.7737 and bedloads tending to have less radiogenic Sr
285 isotopes than suspended loads. These results fall within the large range of Sr isotopes
286 usually measured in the silicate and/or carbonate fractions isolated from Himalayan
287 derived sediments (Harris et al., 1998; Galy et al., 1999; Galy and France-Lanord, 2001;
288 Pierson-Wickmann et al., 2001; Singh et al., 2008). Such radiogenic isotopic compositions

289 are due to the presence of extremely radiogenic sources in the Himalayan mountain
290 range, in particular in the Lesser Himalayan units ($^{87}\text{Sr}/^{86}\text{Sr} > 0.8$; Derry and France-
291 Lanord, 1996; Singh et al., 2008).

292 Sr isotopic compositions measured in the silicate fractions of the suspended load
293 BR 522 and its grain-size fractions are provided in Table 2. The bulk leached suspended
294 load BR 522 shares comparable $^{87}\text{Sr}/^{86}\text{Sr}$ ratios with the other unleached suspended loads
295 from the Ganga River (Table 2). Significant Sr isotopic differences are however observed
296 between the bulk sample and its grain-size fractions with the 2-20 μm fraction being much
297 more radiogenic than the others.

298 **5. Discussion**

299 River sediments are basically mixtures of mineral species. Some minerals, such as
300 quartz, contain virtually no trace elements and their proportion in the sedimentary
301 material influences only the silica content of the sediment but has no impact on most
302 isotopic ratios. In contrast, other minerals very rich in certain trace elements or with very
303 unusual isotopic compositions have the potential to significantly contribute or can even
304 overwhelm the trace element and isotopic budget of river sediments even if they are
305 present in very low proportions. A proper understanding of the role of individual mineral
306 species in the isotopic budget of river sediments thus requires the consideration of
307 several parameters. These include the nature and the proportion of the different mineral
308 species as well as their trace element concentration and isotopic composition.

309 Here, we present Monte-Carlo simulations that quantitatively evaluate the role of
310 individual minerals in the final Nd, Hf, Sr and Pb isotopic budget of river sediments. We
311 simulate the composition of a hundred thousand mixtures between common mineral
312 species that are present in the sedimentary material and that have the potential to

313 significantly influence its isotopic compositions. Then, we compare our results to the data
314 published on bulk sediments.

315 Using mineral proportions estimated by Garzanti et al. (2010; 2011) and calcite
316 contents measured by Lupker et al. (2012) in suspended loads and bedloads from the
317 Ganga River in the Bangladesh delta, we first defined a range of possible proportions for
318 each type of mineral (see Supplementary File). For each mineral species, we then
319 randomly sample proportions within this range and associate them with the Nd, Hf, Sr or
320 Pb concentrations and isotopic compositions measured in our mineral separates. Finally,
321 we calculate the isotopic compositions of the resulting mixtures using the following
322 equation, written here for the Nd isotopic system:

$$323 \quad \left(\frac{^{143}\text{Nd}}{^{144}\text{Nd}} \right)_{\text{mixture}} = \sum_{i=1}^n \left[x_i \cdot \frac{C_{\text{Nd},i}}{C_{\text{Nd},\text{mixture}}} \cdot \left(\frac{^{143}\text{Nd}}{^{144}\text{Nd}} \right)_i \right]$$

324 where n is the number of minerals involved in the mixture; x_i the weight proportion of
325 mineral i sampled randomly in a defined range; $C_{\text{Nd},i}$ and $\left(\frac{^{143}\text{Nd}}{^{144}\text{Nd}} \right)_i$ the Nd content
326 and the Nd isotopic composition of mineral i (see Table 1); and
327 $C_{\text{Nd},\text{mixture}} = \sum_{i=1}^n [x_i \cdot C_{\text{Nd},i}]$, the Nd concentration of the mixture.

328 In the following sections, we compare the modeled Nd, Hf, Sr and Pb isotopic
329 compositions to those measured in both suspended load and bedload sediments as
330 sampled in the Ganga River in the Bangladesh delta (data from the literature and our Sr
331 isotope measurements). Using such approach, we can evaluate the role of each mineral in
332 the isotopic budget of all river sediments. We illustrate the results of our Monte-Carlo
333 simulations for each isotopic system in diagrams that show the contribution of the various
334 mineral species as a function of the modeled isotopic composition for all mixtures. The

335 contribution of each mineral i in the $^{143}\text{Nd}/^{144}\text{Nd}$ budget, for example, is determined in
336 percentage using the following equation:

$$337 \quad \text{Mineral contribution} = 100 \cdot x_i \cdot \frac{C_{\text{Nd},i}}{C_{\text{Nd,mixture}}} \cdot \left(\frac{^{143}\text{Nd}}{^{144}\text{Nd}} \right)_i \bigg/ \left(\frac{^{143}\text{Nd}}{^{144}\text{Nd}} \right)_{\text{mixture}}$$

338 All details about the input parameters, the way simulations were performed and
339 the robustness of the Monte-Carlo results are provided in the Supplementary File. We
340 performed several simulations to assess the sensitivity of our models to the proportions,
341 concentrations and isotopic compositions of the minerals (see Supplementary File). Here,
342 we just emphasize that the simulation results are very well constrained for the four
343 isotopic systems. The contribution of each mineral species in the whole-rock isotopic
344 budgets remains quite constant even if we introduce large errors on the input parameters,
345 such as the mineral proportions or the concentrations and isotopic compositions of
346 mineral species. An important implication is that the results presented in this study may
347 be valid not only for the Ganga sediments, but also for any sediment sampled in other
348 large river systems all over the world.

349

350 **5.1. Which minerals control Nd isotopes of river sediments?**

351 To perform the Monte-Carlo simulation modeling Nd isotopic compositions of
352 sediments, we considered the 14 analyzed minerals (K-feldspar, plagioclase, muscovite,
353 biotite, magnetite, zircon, titanite, apatite, monazite/allanite, amphibole, epidote, garnet,
354 carbonate, and clay) and we set the mineral proportions within the range known for river
355 sediments sampled in the Bangladesh delta (see Supplementary File and inset in Figure
356 3). Results are shown in Figure 3 while $^{143}\text{Nd}/^{144}\text{Nd}$ for the most important mineral
357 phases are shown along the horizontal axis.

358 The first important observation is that minerals that significantly contribute to the
359 Nd isotopic budget are very few: monazite/allanite, clay, titanite and biotite. All other
360 minerals (K-feldspars, plagioclase, muscovite, magnetite, zircon, apatite, amphibole,
361 epidote, garnet, and carbonate) always contribute to less than 10% of the isotopic budget,
362 over the entire range of modeled Nd isotopic compositions; this is why they are not shown
363 in Figure 3. Because of its extreme enrichment in Nd (Figure 2), the monazite/allanite
364 fraction entirely dominates the Nd isotopic budget of modeled mixtures and it can even
365 control 100% of the isotopic budget (Figure 3) while its proportion in the mineral
366 assemblage never exceeds 0.5 wt.% (see Supplementary File and inset of Figure 3). It is
367 only when the modeled Nd isotopic composition is greater than 0.51185 that the
368 contribution of clay, titanite and biotite starts to surpass that of monazite and allanite
369 (Figure 3).

370 As shown by the grey band in Figure 3, Nd isotopic ratios reported for bedloads
371 and suspended loads sampled at the outflow of the Ganga span a limited range of values
372 between 0.51172 and 0.51179 (Garçon et al., 2013a), values similar to those reported by
373 Galy and France-Lanord (2001) for sediments sampled at the same location. According to
374 our simulation (Figure 3), such compositions correspond to mixtures highly dominated
375 by monazite and allanite (60-100%) with a small but significant contribution from clays
376 (0-30%). We can therefore suggest that the few monazite and allanite grains present in
377 the sediments (<0.5 wt%, see Supplementary File) totally overwhelm the Nd isotopic
378 compositions of river sediments in the Bangladesh delta.

379 In a more classical diagram showing $^{143}\text{Nd}/^{144}\text{Nd}$ ratios as a function of
380 $^{147}\text{Sm}/^{144}\text{Nd}$ ratios (Figure 4), it becomes even more obvious that the unradiogenic Nd
381 isotopic signature of the monazite/allanite fraction is the controlling factor of the
382 composition of the Ganga sediments since no other mineral has a Nd isotopic composition

383 similar to or lower than that of the bulk sediments. As suggested by our Monte-carlo
384 simulation, both bedloads and suspended loads are well reproduced by a mixture of
385 monazite, allanite, clay \pm biotite, titanite (Figure 4).

386

387 **5.2. Which minerals control Hf isotopes of river sediments?**

388 The results of the Monte-Carlo simulation for Hf isotopes are shown in Figure 5
389 together with the results obtained on the various mineral separates. Eleven minerals
390 were introduced in the simulation: K-feldspar, plagioclase, muscovite, biotite, magnetite,
391 zircon, titanite, amphibole, epidote, garnet, and clay. Quartz and carbonates were ignored
392 because they do not contain any Hf and we did not measure their Hf isotopic
393 compositions. The monazite/allanite fraction and the apatite fraction were also ignored
394 because they contain a lot of small zircons, a feature that explains their unusually high Zr-
395 Hf concentrations compared to what is commonly measured in such minerals (Ayres and
396 Harris, 1997). We suggest, therefore, that if we had measured their Hf isotopic
397 compositions, the results would not have been representative of the composition of the
398 monazite, allanite or the apatite but would have reflected that of the zircons present in
399 the fractions.

400 As for Nd isotopes, only few minerals significantly contribute to the Hf isotopic
401 budget of the modeled mixtures: zircon, clay, muscovite, biotite and titanite. By contrast,
402 garnet, amphibole, epidote, magnetite, plagioclase, and K-feldspar contribute to less than
403 10% of the Hf isotopic budget and are not shown in Figure 5. Modeled Hf isotopic
404 compositions span a relatively large range of values between 0.28197 and 0.28235. One
405 of the most remarkable features is that unradiogenic Hf-rich zircon totally buffers the Hf
406 isotopic budget over a large range of isotopic compositions (Figure 5) while its proportion

407 in the mineral assemblage is always less than 0.5 wt% (see Supplementary File and inset
408 of Figure 5). Clay is the second important mineral but its contribution never exceeds 50%.
409 Together with muscovite, biotite and titanite, the clay fraction accounts for the most
410 radiogenic Hf isotopic compositions in the simulation.

411 In contrast to Nd, there is a difference between the $^{176}\text{Hf}/^{177}\text{Hf}$ ratio of bedloads and
412 suspended loads sampled at the outflow of the Ganga River (Garçon et al., 2012; 2013a).
413 As shown by grey bands in Figure 5, bedloads are less radiogenic than suspended loads.
414 The results of our Monte-carlo simulation show that the difference is easily explained by
415 different contributions of unradiogenic zircon. The range of $^{176}\text{Hf}/^{177}\text{Hf}$ measured in
416 bedloads results from a very high contribution of zircon (i.e. 70-100% of their Hf isotopic
417 budget) and the relative contribution of all other minerals remains always below 15%.
418 The higher $^{176}\text{Hf}/^{177}\text{Hf}$ measured in suspended loads results from a higher contribution
419 of more radiogenic minerals such as clay, muscovite, biotite and titanite and a lower
420 contribution of zircon, even if it can still contribute to up to 50% of the isotopic budget
421 (Figure 5).

422 In Figure 6, we show the relationship between $^{176}\text{Hf}/^{177}\text{Hf}$ and $1/\text{Hf}$ for minerals,
423 bedloads and suspended loads. In contrast to what we did for the Nd case, we chose to not
424 represent Hf isotopic compositions as a function of their parent/daughter ratios (i.e.
425 $^{176}\text{Lu}/^{177}\text{Hf}$ ratios) because Lu and Hf are not carried by the same minerals and it would
426 introduce confusion when evaluating the role of individual minerals in the Hf isotopic
427 compositions of sediments. We also normalized the $1/\text{Hf}$ ratio of all sediments to the SiO_2
428 content of the clay fraction (see footnote of Figure 6 for more details), because dilution by
429 variable amounts of quartz has a drastic effect on the Hf concentration of river sediments.
430 As highlighted by our Monte-Carlo simulations, Figure 6 shows clearly that all bedloads
431 plot close to zircon, confirming that this mineral buffers the Hf isotopic budget of

432 bedloads. The composition of suspended loads requires a mixture of more radiogenic
433 minerals such as biotite, muscovite and clay together with less radiogenic titanite and
434 zircon for some of them (Figure 6).

435

436 **5.3. Which minerals control Sr isotopes of river sediments?**

437 In Figure 7a, we show $^{87}\text{Sr}/^{86}\text{Sr}$ measured on the various minerals and the modeled
438 $^{87}\text{Sr}/^{86}\text{Sr}$ for mixing simulations between K-feldspar, plagioclase, muscovite, biotite,
439 magnetite, zircon, titanite, amphibole, epidote, garnet, carbonate, and clay. Six minerals
440 (garnet, amphibole, titanite, zircon, magnetite, and biotite) are not shown in the figure
441 because they all are minor contributors (<10%) to the Sr isotopic budget. In contrast,
442 because of their high Sr contents (Table 1), epidote, K-feldspar, plagioclase, carbonate
443 and, to a lesser extent, clay, and muscovite exert a major role on the $^{87}\text{Sr}/^{86}\text{Sr}$ of the
444 modeled mixtures.

445 The range of Sr isotopic compositions measured in bedloads and suspended loads
446 from the Ganga River is shown by grey bands in Figure 7a. Variations of $^{87}\text{Sr}/^{86}\text{Sr}$ ratios
447 as a function of $1/\text{Sr}$ are reported in Figure 8. Figure 7a demonstrates clearly that our
448 Monte-Carlo simulation fails in reproducing the high $^{87}\text{Sr}/^{86}\text{Sr}$ of all sediments, in
449 particular those of suspended loads. We can think of several possible reasons to explain
450 the mismatch between modeled and measured Sr isotope ratios.

451 The first possibility is that we have missed a component/mineral with high $^{87}\text{Sr}/^{86}\text{Sr}$
452 and high Sr content in our Monte-Carlo procedure. The missing component cannot be
453 dissolved Sr, or Sr carried by small particles (< 0.2 μm) because all suspended loads were
454 filtered under pressure at 0.2 μm (Lupker et al., 2011) and the filtered fractions
455 containing particles smaller than 0.2 μm were not analyzed in this study. As a

456 consequence, dissolved ions and very fine particles cannot participate to the Sr isotopic
457 budget of suspended loads. Even if we assume that the filtration was not complete, the Sr
458 isotopic composition of these fractions (clay < 2 μ m at 0.747 and river water with
459 $^{87}\text{Sr}/^{86}\text{Sr} < 0.73$, see Table 1 and Galy et al., 1999) are less radiogenic than the sediments,
460 hence they cannot constitute the missing components with high $^{87}\text{Sr}/^{86}\text{Sr}$ ratios. Given
461 their high Sr contents (Table 1), potential other candidates are apatite and
462 monazite/allanite. However, these minerals have low $^{87}\text{Rb}/^{86}\text{Sr}$ ratios, just like carbonate
463 and epidote that have the lowest $^{87}\text{Sr}/^{86}\text{Sr}$ ratios (Figure 8). It seems thus unlikely that
464 these phases could have the elevated $^{87}\text{Sr}/^{86}\text{Sr}$ that is required to explain the observed
465 mismatch between model and measurements. Adding these mineral phases in the
466 simulations would probably even make the modeled Sr isotopic compositions less
467 radiogenic.

468 A second possibility is that we underestimated the proportions of very radiogenic
469 minerals, such as muscovite or biotite (Figure 8), in the fine suspended loads. However,
470 as shown in details in the Supplementary File, the results of the Monte-Carlo simulations
471 are robust and the range of modeled Sr isotopic compositions remains incompatible with
472 the measured values even with very different mineral proportions.

473 The last possibility is that one or several mineral phases that contribute significantly
474 to the Sr isotopic budget have $^{87}\text{Sr}/^{86}\text{Sr}$ ratios higher than the value that we measured.
475 We suspect that it could be the case for K-feldspar and muscovite for the following reason:
476 for convenience, we separated these two minerals from the coarsest fraction (>250 μ m)
477 of bedload BR 717 (see section 3.1) and we suspect that smaller minerals might have
478 different isotopic compositions. Indeed, large ranges of $^{87}\text{Sr}/^{86}\text{Sr}$ are reported for K-
479 feldspar (0.737 to 0.801) and muscovite (0.765 to 8.353) in the Himalayan rocks (Mehta,
480 1977; Kai, 1981; Ferrara et al., 1983; Deniel et al., 1987; Johnson and Rogers, 1997) and

481 we believe that the coarse feldspar and muscovite that we isolated ($^{87}\text{Sr}/^{86}\text{Sr}$ of 0.7587
482 and 0.8313, respectively) might have lower $^{87}\text{Sr}/^{86}\text{Sr}$ than grains present in fine
483 suspended loads.

484 Analyses of finer K-feldspar and muscovite fractions would help support this
485 hypothesis but the separation and purification of a significant amount of fine minerals
486 constitute a difficult technical challenge. As an alternative, we performed additional Sr
487 isotopic analyses on several grain-size fractions separated from a Ganga suspended load
488 sampled in the Bangladesh delta (sample BR 522; Figure 1, Table 2). These analyses were
489 carried out on the silicate part of the samples to establish whether the Sr isotopic
490 compositions of the silicate minerals could vary as a function of mineral grain-size.
491 Results clearly indicate that the grain-size fractions do not have the same Sr isotopic
492 composition as the bulk sample and span a relatively large range of values from 0.7575 to
493 0.7824 (Table 2). Interestingly, the 2-20 μm fraction, representing almost half of the
494 suspended load sample (see Table 2), has the most radiogenic Sr isotopic composition,
495 supporting the idea that finer K-feldspars and muscovites may be more radiogenic than
496 the coarse minerals that we analyzed. This could occur if fine K-feldspars and muscovites
497 were older than coarse ones. Calculations show that an age difference of only 50-70 Ma is
498 sufficient to increase the $^{87}\text{Sr}/^{86}\text{Sr}$ ratio of muscovite from 0.8 to 1.0 assuming a $^{87}\text{Rb}/^{86}\text{Sr}$
499 ratio of 200-300, values commonly measured in Himalayan muscovite (e.g. Mehta, 1977;
500 Kai, 1981; Ferrara et al., 1983; Deniel et al., 1987; Johnson and Rogers, 1997). The age
501 difference required to increase the $^{87}\text{Sr}/^{86}\text{Sr}$ ratio of K-feldspar from 0.76 to 0.80 is of
502 course higher (about 150 Ma) because $^{87}\text{Rb}/^{86}\text{Sr}$ is usually around 20 (e.g. Ferrara et al.,
503 1983; Deniel et al., 1987; Johnson and Rogers, 1997). Another possibility is that the fine
504 K-feldspars and muscovites had initially crystallized with high Rb but similar Sr contents,
505 leading to higher Rb/Sr ratios than the ratio measured in the coarse minerals, and leading

506 in turn, to more radiogenic Sr isotopic compositions over the same amount of time.
507 Unfortunately, available data are not sufficient to constrain the origin of the observed
508 isotopic variability as a function of grain-size and further work is needed to understand
509 this feature.

510 In order to reproduce the isotopic compositions measured on whole-rock
511 sediments, we revised the Monte-Carlo simulation assuming that K-feldspars and
512 muscovites had more radiogenic Sr isotopic compositions but similar Sr concentrations.
513 The results of the simulation using $^{87}\text{Sr}/^{86}\text{Sr}$ ratios of 0.800 for K-feldspar (instead of
514 0.7587) and 1.0 for muscovite (instead of 0.8313) are shown in Figure 7b. In this case, the
515 simulated mixtures overlap with the fields known for bedloads and suspended loads. As
516 in the first simulation (Figure 7a), K-feldspar, carbonate, clay, plagioclase, epidote and
517 muscovite control the Sr isotopic budget of sediments (Figure 7b). Assuming that the
518 revised simulation is valid, isotopic differences between bedloads and suspended loads
519 could be explained by higher relative contributions of epidote and carbonate in bedloads
520 and muscovite/K-feldspar in suspended loads.

521

522 **5.4. Which minerals control Pb isotopes of river sediments?**

523 To perform the Monte-Carlo simulation for Pb isotopes, we used the data already
524 published by Garçon et al. (2013b) but we list them for convenience in Table 1. Because
525 we did not measure the Pb isotopic composition of all the mineral fractions, we used an
526 estimated value for the “heavy mineral” fraction, containing zircon, monazite and allanite,
527 to perform our simulation (i.e. $^{206}\text{Pb}/^{204}\text{Pb}$ ratio of about 800-900 after Garçon et al.,
528 2013b). As we obtained similar results for $^{208}\text{Pb}/^{204}\text{Pb}$, $^{207}\text{Pb}/^{204}\text{Pb}$ and $^{206}\text{Pb}/^{204}\text{Pb}$ ratios,
529 only the results obtained for $^{206}\text{Pb}/^{204}\text{Pb}$ ratios are shown in Figure 9. Seven minerals

530 (biotite, magnetite, titanite, amphibole, epidote, garnet and carbonate) always contribute
531 to less than 10% to the Pb isotopic budget and are not shown in Figure 9. In contrast, clay,
532 K-feldspar, muscovite, plagioclase and zircon/monazite/allanite contribute significantly
533 to the final isotopic composition. The modeled $^{206}\text{Pb}/^{204}\text{Pb}$ cover a very large range of
534 values between 19 and 55, the highest values being associated with high contributions of
535 zircon, monazite and allanite in the mixture (Figure 9). Indeed, if we perform a simulation
536 without these heavy minerals, the modeled $^{206}\text{Pb}/^{204}\text{Pb}$ ratios only range between 19.0
537 and 19.8. This is because zircon, monazite and allanite are extremely radiogenic
538 (estimated $^{206}\text{Pb}/^{204}\text{Pb}$ ratio of 800-900; Garçon et al., 2013b), and even a minute amount
539 of this mineral mixture in the sediment ($\leq 1\text{wt}\%$) significantly shifts the modeled Pb
540 isotopic compositions towards very radiogenic values (Figure 9).

541 The ranges of $^{206}\text{Pb}/^{204}\text{Pb}$ measured for bedloads (20.6-22.2) and suspended loads
542 (19.8-20.1) are shown using grey bands in Figure 9. Our results show that for both types
543 of sediments, the Pb-rich clay and K-feldspar control up to 80% of the Pb isotopic budget
544 while muscovite and plagioclase are other significant contributors. Our simulations also
545 show that zircon, monazite and allanite play a key role in increasing the Pb isotopic
546 compositions of both bedloads and suspended loads. Indeed, if these heavy minerals were
547 not present, the $^{206}\text{Pb}/^{204}\text{Pb}$ ratio of any mixture could not exceed 19.8, a value
548 significantly lower than what is measured on both bedloads and suspended loads. This
549 implies that the Pb isotopic budget of both bedloads and suspended loads are influenced
550 by a “heavy mineral effect”, with a stronger impact on bedloads than on suspended loads
551 (see Figure 9 and Garçon et al. (2013b) for further discussion).

552

553 **5.5. Geological implications**

554 We showed above that the difference in Hf, Sr and Pb isotopic compositions
555 between bedloads and suspended loads sampled at the same location are due to different
556 mineral contributions that are ultimately controlled by mineral sorting processes within
557 the water column. We now evaluate the implications of these results for (1) sediment
558 provenance studies based on isotope data and (2) large-scale isotopic partitioning
559 between continental and oceanic sediments.

560

561 **5.5.1. Sediment provenance studies**

562 Isotopic data are often used to trace erosion distribution in watersheds (e.g., Galy
563 and France-Lanord, 2001; Clift et al., 2002; Singh and France-Lanord, 2002; Singh et al.,
564 2008) as well as changes through time of the source of sedimentary material in relation
565 to changes of tectonic regimes and/or climate (e.g. Walter et al., 2000; Gingele et al., 2007;
566 Yan et al., 2007; Haley et al., 2008; Singh et al., 2008; Cina et al., 2009; Rahaman et al.,
567 2009; Stumpf et al., 2011; Hu et al., 2012). They are also largely used in studies focusing
568 on the changes of ocean circulation through time (Revel et al., 1996; Innocent et al., 1997;
569 Stille et al., 1997; Bayon et al., 2002; Frank, 2002; Goldstein and Hemming, 2003;
570 Piotrowski et al., 2004; Gourlan et al., 2008; Haley et al., 2008; Ehlert et al., 2011) or in
571 studies that attempt to establish average isotopic compositions or ages for large areas of
572 continental crust (Goldstein et al., 1984; Goldstein and Jacobsen, 1988; Asmerom and
573 Jacobsen, 1993; Allègre et al., 1996; Millot et al., 2004; Kamber et al., 2005; Dhuime et al.,
574 2011). It is therefore important to know which isotopic systems are robust tracers of
575 source compositions and in which conditions.

576 Nd isotopes are certainly an important source tracer. Our study of bedloads,
577 suspended loads and individual minerals confirms that it is robust. More specifically, we
578 demonstrate that the isotopic budget of both suspended loads and bedloads is buffered
579 by monazite and allanite even though these minerals are present in extremely small
580 proportions (< 0.5 wt.%) in the sediments. Both types of sediments can be used for
581 provenance studies. We also confirm the conclusions presented by Garçon et al. (2011)
582 who demonstrated that, in beach placers, monazite by itself was a good proxy to estimate
583 the Nd isotopic composition of large continental areas. Analyses of populations of
584 monazite grains or analyses of single grains could be an alternative to whole rock
585 measurements.

586 Hf isotopic analysis of zircon grains is another widely used approach to trace source
587 compositions (Bodet and Schärer, 2000; Davis et al., 2005; Harrison et al., 2005; Veevers
588 et al., 2005; Flowerdew et al., 2006; Hawkesworth and Kemp, 2006; Kemp et al., 2007;
589 Zeh et al., 2007; Belousova et al., 2010). Using the $^{176}\text{Hf}/^{177}\text{Hf}$ of bulk sediments as source
590 tracer is definitively trickier in view of the “zircon effect” highlighted by previous studies
591 (Patchett et al., 1984; Vervoort et al., 1999; Chauvel et al., 2008; Bayon et al., 2009;
592 Carpentier et al., 2009; Vervoort et al., 2011). However, our study demonstrates and
593 quantifies the fact that since zircon almost entirely controls the $^{176}\text{Hf}/^{177}\text{Hf}$ ratio of
594 bedloads, these sediments can be used for source provenance studies. In contrast,
595 suspended loads that are depleted in zircon and have their Hf isotopic budget controlled
596 by radiogenic minerals such as biotite, muscovite, clay, or amphibole, have isotopic
597 compositions that differ from that of their source and cannot be used to trace sediment
598 provenance.

599 A surprising feature is that heavy minerals not only affect the Hf isotopic
600 compositions of river sediments but also have dramatic effects on their Pb isotopic

601 compositions. Indeed, our calculations indicate that, because of their extremely
602 radiogenic Pb isotopes, zircon, monazite and allanite have the potential to significantly
603 increase the Pb isotopic ratios of both bedloads and suspended loads (e.g., as high as 60
604 for $^{206}\text{Pb}/^{204}\text{Pb}$; Figure 9). Garçon et al. (2013) have shown that mineralogical sorting
605 processes during fluvial transport lead to an excess concentration of heavy minerals in
606 bedloads and, to lesser extent, in suspended loads. This “heavy mineral effect” shifts the
607 Pb isotopic compositions of most river sediments, including some suspended loads,
608 towards more radiogenic values than their source areas. The best approach to constrain
609 the Pb isotopic composition of the source areas is thus to concentrate on K-feldspars or
610 clays separated from sediments because these fractions contain most of the lead initially
611 present in crustal rocks and are almost not affected by the “heavy mineral effect” (see
612 Garçon et al., 2013b for further discussion).

613 Finally, using Sr isotopes in river sediments to trace the composition of source areas
614 appears very difficult without taking into account potential bias due to mineralogical
615 sorting processes during sediment transport. Bedloads and suspended loads have
616 different isotopic compositions and, according to our calculations, the more radiogenic Sr
617 signature of suspended loads compared to bedloads probably comes from higher
618 contributions of radiogenic muscovite and/or K-feldspar in suspended loads (Figure 7)
619 together with higher contributions of less radiogenic epidote and carbonate in bedloads.
620 It remains unclear whether either bedloads or suspended loads have compositions
621 similar to that of the source areas. As a consequence, Sr isotopes can only be used as a
622 source proxy if the sources are isotopically extremely different (i.e. range larger than that
623 created by mineralogical sorting processes), as is rarely the case but occurs in the
624 Himalayan system.

625

626 **5.5.2. Difference between what goes into the deep ocean and what**
627 **remains on continents**

628 At a global scale, mineral sorting processes are responsible for significant isotopic
629 fractionation between continental sediments and terrigenous oceanic clays. Patchett et
630 al. (1984) were the first to discuss such effects and showed their impact on the Hf isotopic
631 systematics of sediments. They argued that the “zircon effect”, i.e. retention of
632 unradiogenic Hf-rich zircons on continents, led to the delivery into the oceans of finer
633 detrital material, poor in zircons and with radiogenic Hf isotopes. Numerous other studies
634 confirmed the observation since 1984 (Chauvel et al., 2008; Bayon et al., 2009; Carpentier
635 et al., 2009; Chauvel et al., 2009; Vervoort et al., 2011). Recently, Garçon et al. (2012;
636 2013a) showed that almost half of the bias towards radiogenic Hf isotopic seen today in
637 terrigenous oceanic clays is observed in suspended river sediments on continents. The
638 Hf Monte-Carlo simulation presented in Figure 5 confirms that suspended loads delivered
639 at the mouth of a river as large as the Ganga still contain zircons. In particular, we show
640 that, even if radiogenic minerals such as phyllosilicates contribute to a non-negligible part
641 of the Hf isotopic composition of the Ganga suspended loads, zircon can still control up to
642 50% of their Hf isotopic budget (Figure 5). Thus, further sorting must occur in the oceanic
643 environment to reach the maturity of terrigenous oceanic clay and their characteristic
644 highly radiogenic zircon-free Hf signature. This sorting could occur in the ocean, next to
645 the continental margins due to a rapid change of the hydrodynamic conditions (Lisitzin,
646 1996; Stummeyer et al., 2002).

647 Deposition of heavy minerals in the coastal zone is probably a key process that not
648 only affects the Hf isotopic composition of sedimentary material delivered to the ocean,
649 but also affects their Pb and Sr isotopes in a similar way. Our simulations demonstrate
650 that the Pb isotopic composition of bedloads and even that of suspended loads are biased

651 towards radiogenic values by a “heavy mineral effect”. Thus, we expect terrigenous
652 oceanic clays to be characterized by less radiogenic Pb isotopic ratios than river
653 suspended loads. Similarly, the deposition of dense epidote and/or coarse particles in
654 coastal zones should lead to the delivery into the deep oceans of materials with more
655 radiogenic Sr isotopic compositions than river suspended loads. Such a potential Sr
656 isotopic fractionation at the land/ocean interface has already been pointed out by
657 Eisenhauer et al. (1999) and our calculations confirm their suggestions. Finally,
658 deposition of heavy monazite and allanite in the coastal zone should not modify the Nd
659 isotopic composition of sediments delivered in the deep ocean, since these two minerals
660 have essentially the same $^{147}\text{Sm}/^{144}\text{Nd}$ as both bulk sediments and continental sources
661 (Patchett et al., 1984; McLennan, 1989; Garçon et al., 2011; Vervoort et al., 2011).

662 **6. Summary and Conclusions**

663 The Monte-Carlo simulations performed in this study provide a framework to
664 decipher the contribution of individual mineral species to the Nd, Hf, Sr and Pb isotopic
665 budget of river sediments. They also provide clues to understand the isotopic differences
666 observed between bedloads and suspended loads that are related to mineral sorting
667 processes during the fluvial transport of sediments. The results of the Monte-Carlo
668 simulations are well constrained and could be used to understand the isotopic
669 systematics of other sediments from large river systems all over the world.

670 An important result is that, despite the diversity of mineral species present in river
671 sediments, only a few minerals really participate in the Nd, Hf, Sr and Pb isotopic budgets.
672 Nd isotopes of both bedloads and suspended loads are mainly controlled by monazite and
673 allanite and they are not modified by mineral sorting processes. Hence, they can be used
674 to trace the continental sources of sediments. By contrast, mineral sorting processes lead

675 to significant Hf, Sr and Pb isotopic diversity. We demonstrate that the Hf isotopic budget
676 of bedloads is totally dominated by the contribution of unradiogenic Hf-rich zircons. The
677 more radiogenic Hf signature of suspended loads results from lower but still significant
678 contribution of zircons combined to higher contributions of more radiogenic minerals
679 such as phyllosilicates. The Pb isotopic budget of all river sediments is dominated by K-
680 feldspar and clay contributions but it is also significantly affected by a “heavy mineral
681 effect” that deviates the Pb isotopic compositions towards very radiogenic values. Sr
682 isotopes in river sediments are more difficult to model but they are mainly controlled by
683 K-feldspar, plagioclase, muscovite, carbonate, clay and epidote with a systematic
684 difference between bedloads and suspended loads.

685 Because isotopic fractionations caused by mineral sorting processes during
686 sediment transport can be very large, we stress the need for caution when using the
687 isotopic compositions of river sediments as provenance proxies. Of the four isotopic
688 systems studied here, Nd is this only one that is not affected by the mineralogical effects.
689 We anticipate that hydrodynamic sorting in the coastal zone should further fractionate
690 the Hf, Sr and Pb isotopic systems in terrigenous oceanic sediments. In particular, the
691 deposition of heavy minerals at the river/ocean interface could lead to the delivery into
692 the deep ocean of sediments with even higher $^{176}\text{Hf}/^{177}\text{Hf}$ and $^{87}\text{Sr}/^{86}\text{Sr}$ and lower Pb
693 isotopic ratios than river suspended loads. Further studies on the isotopic variability of
694 terrigenous oceanic sediments are needed to better constrain the impact of mineral
695 sorting in the oceanic environment and its role on the decoupling of isotopic systems at a
696 large scale.

697

698 **Acknowledgments**

699 We would like to thank A. Galy, V. Galy and M. Lupker for sample collection, S. Andò
700 for his help during mineral separation, S. Bureau and C. Poggi for their help in the clean
701 lab, P. Telouk and P. Nonnotte for assistance during isotopic measurements in Lyon and
702 Brest, as well as N.T. Arndt and E. Lewin for constructive discussions that helped to
703 develop and interpret the results of the Monte-Carlo simulations. We also greatly thank
704 the editor Laurie Reisberg and the two reviewers, Jeff Vervoort and Bill White, who made
705 very constructive comments that certainly improve the content of this manuscript. This
706 study was supported by fundings from CNRS and INSU programs.

707

708 **References**

- 709 Allègre, C.J., Dupré, B., Nègre, P., Gaillardet, J., 1996. Sr-Nd-Pb isotope systematics in
710 Amazon and Congo River systems: constraints about erosion processes. *Chemical*
711 *Geology* 131, 93–112.
- 712 Asmerom, Y., Jacobsen, S.B., 1993. The Pb isotopic evolution of the Earth: inferences from
713 river water suspended loads. *Earth and Planetary Science Letters* 115, 245–256.
- 714 Ayres, M., Harris, N., 1997. REE fractionation and Nd-isotope disequilibrium during
715 crustal anatexis: constraints from Himalayan leucogranites. *Chemical Geology* 139,
716 249–269.
- 717 Bayon, G., Burton, K.W., Soulet, G., Vigier, N., Dennielou, B., Etoubleau, J., Ponzevera, E.,
718 German, C.R., Nesbitt, R.W., 2009. Hf and Nd isotopes in marine sediments:
719 Constraints on global silicate weathering. *Earth and Planetary Science Letters* 277,
720 318–326.
- 721 Bayon, G., German, C.R., Boella, R.M., Milton, J.A., Taylor, R.N., Nesbitt, R.W., 2002. An
722 improved method for extracting marine sediment fractions and its application to Sr
723 and Nd isotopic analysis. *Chemical Geology* 187, 179–199.
- 724 Bea, F., 1996. Residence of REE, Y, Th and U in granites and crustal protoliths; implications
725 for the chemistry of crustal melts. *Journal of Petrology* 37, 521–552.
- 726 Belousova, E.A., Kostitsyn, Y.A., Griffin, W.L., Begg, G.C., O'reilly, S.Y., Pearson, N.J., 2010.
727 The growth of the continental crust: Constraints from zircon Hf-isotope data. *Lithos*
728 119, 457–466.
- 729 Bodet, F., Schärer, U., 2000. Evolution of the SE-Asian continent from U-Pb and Hf isotopes

730 in single grains of zircon and baddeleyite from large rivers. *Geochimica et*
731 *Cosmochimica Acta* 64, 2067–2091.

732 Bouchez, J., Gaillardet, J., France-Lanord, C., Maurice, L., Dutra-Maia, P., 2011. Grain size
733 control of river suspended sediment geochemistry: Clues from Amazon River depth
734 profiles. *Geochem. Geophys. Geosyst.* 12, Q03008.

735 Carpentier, M., Chauvel, C., Maury, R.C., Mattielli, N., 2009. The “zircon effect” as recorded
736 by the chemical and Hf isotopic compositions of Lesser Antilles forearc sediments.
737 *Earth and Planetary Science Letters* 287, 86–99.

738 Chauvel, C., Blichert-Toft, J., 2001. A hafnium isotope and trace element perspective on
739 melting of the depleted mantle. *Earth and Planetary Science Letters* 190, 137–151.

740 Chauvel, C., Bureau, S., Poggi, C., 2011. Comprehensive chemical and isotopic analyses of
741 basalt and sediment reference materials. *Geostandards and Geoanalytical Research*
742 35, 125–143.

743 Chauvel, C., Lewin, E., Carpentier, M., Arndt, N.T., Marini, J.-C., 2008. Role of recycled
744 oceanic basalt and sediment in generating the Hf–Nd mantle array. *Nature*
745 *Geosciences* 1, 64–67.

746 Chauvel, C., Marini, J.-C., Plank, T., Ludden, J.N., 2009. Hf–Nd input flux in the Izu–Mariana
747 subduction zone and recycling of subducted material in the mantle. *Geochem.*
748 *Geophys. Geosyst.* 10, Q01001.

749 Cina, S.E., Yin, A., Grove, M., Dubey, C.S., Shukla, D.P., Lovera, O.M., Kelty, T.K., Gehrels, G.E.,
750 Foster, D.A., 2009. Gangdese arc detritus within the eastern Himalayan Neogene
751 foreland basin: Implications for the Neogene evolution of the Yalu–Brahmaputra
752 River system. *Earth and Planetary Science Letters* 285, 150–162.

753 Clift, P.D., Lee, J.I., Hildebrand, P., Shimizu, N., Layne, G.D., Blusztajn, J., Blum, J.D., Garzanti,
754 E., Khan, A.A., 2002. Nd and Pb isotope variability in the Indus River System:
755 implications for sediment provenance and crustal heterogeneity in the Western
756 Himalaya. *Earth and Planetary Science Letters* 200, 91–106.

757 Davis, D.W., Amelin, Y., Nowell, G.M., Parrish, R.R., 2005. Hf isotopes in zircon from the
758 western Superior province, Canada: Implications for Archean crustal development
759 and evolution of the depleted mantle reservoir. *Precambrian Research* 140, 132–156.

760 Deniel, C., Vidal, P., Fernandez, A., Fort, P., Peucat, J.J., 1987. Isotopic study of the Manaslu
761 granite (Himalaya, Nepal): inferences on the age and source of Himalayan
762 leucogranites. *Contrib Mineral Petrol* 96, 78–92.

763 Derry, L.A., France-Lanord, C., 1996. Neogene Himalayan weathering history and river
764 $^{87}\text{Sr}/^{86}\text{Sr}$: impact on the marine Sr record. *Earth and Planetary Science Letters* 142,
765 59–74.

766 Dhuime, B., Hawkesworth, C.J., Storey, C.D., Cawood, P.A., 2011. From sediments to their
767 source rocks: Hf and Nd isotopes in recent river sediments. *Geology* 39, 407–410.

768 Ehlert, C., Frank, M., Haley, B.A., Böniger, U., De Deckker, P., Gingele, F.X., 2011. Current
769 transport versus continental inputs in the eastern Indian Ocean: Radiogenic isotope
770 signatures of clay size sediments. *Geochem. Geophys. Geosyst.* 12, Q06017.

771 Eisenhauer, A., Meyer, H., Rachold, V., Tütken, T., Wiegand, B., Hansen, B.T., Spielhagen,
772 R.F., Lindemann, F., Kassens, H., 1999. Grain size separation and sediment mixing in

773 Arctic Ocean sediments: evidence from the strontium isotope systematic. *Chemical*
774 *Geology* 158, 173–188.

775 Ferrara, G., Tonarini, S., Lombardo, B., 1983. Rb/Sr geochronology of granites and gneisses
776 from the Mount Everest region, Nepal Himalaya. *Int J Earth Sci (Geol Rundsch)* 72,
777 119–136.

778 Flowerdew, M.J., Millar, I.L., Vaughan, A.P.M., Horstwood, M.S.A., Fanning, C.M., 2006. The
779 source of granitic gneisses and migmatites in the Antarctic Peninsula: a combined U–
780 Pb SHRIMP and laser ablation Hf isotope study of complex zircons. *Contrib Mineral*
781 *Petrol* 151, 751–768.

782 Frank, M., 2002. Radiogenic isotopes: Tracers of past ocean circulation and erosional
783 input. *Reviews of Geophysics* 40, 1001.

784 Galy, A., France-Lanord, C., 2001. Higher erosion rates in the Himalaya: Geochemical
785 constraints on riverine fluxes. *Geology* 29, 23–26.

786 Galy, A., France-Lanord, C., Derry, L.A., 1999. The strontium isotopic budget of Himalayan
787 Rivers in Nepal and Bangladesh. *Geochimica et Cosmochimica Acta* 63, 1905–1925.

788 Galy, V., France-Lanord, C., Lartiges, B., 2008. Loading and fate of particulate organic
789 carbon from the Himalaya to the Ganga–Brahmaputra delta. *Geochimica et*
790 *Cosmochimica Acta* 72, 1767–1787.

791 Garçon, M., Chauvel, C., Bureau, S., 2011. Beach placer, a proxy for the average Nd and Hf
792 isotopic composition of a continental area. *Chemical Geology* 287, 182–192.

793 Garçon, M., 2012. Variabilité chimique et isotopique causée par les processus
794 sédimentaires dans les sédiments de rivières Himalayennes, PhD thesis, Grenoble
795 University, France.

796 Garçon, M., Chauvel, C., France-Lanord, C., 2013a. Sedimentary processes decouple Nd and
797 Hf isotopes in river sediments on continents. *Geochimica et Cosmochimica Acta* 121,
798 177–195.

799 Garçon, M., Chauvel, C., France-Lanord, C., Limonta, M., Garzanti, E., 2013b. Removing the
800 "heavy mineral effect" to obtain a new Pb isotopic value for the upper crust.
801 *Geochemistry Geophysics Geosystems* 14, 9, doi: 10.1002/ggge.20219.

802 Garzanti, E., Andò, S., France-Lanord, C., Censi, P., Pietro Vignola, Galy, V., Lupker, M., 2011.
803 Mineralogical and chemical variability of fluvial sediments 2. Suspended-load silt
804 (Ganga–Brahmaputra, Bangladesh). *Earth and Planetary Science Letters* 302, 107–
805 120.

806 Garzanti, E., Andò, S., France-Lanord, C., Vezzoli, G., Censi, P., Galy, V., Najman, Y., 2010.
807 Mineralogical and chemical variability of fluvial sediments 1. Bedload sand (Ganga–
808 Brahmaputra, Bangladesh). *Earth and Planetary Science Letters* 299, 368–381.

809 Garzanti, E., Andò, S., Vezzoli, G., 2008. Settling equivalence of detrital minerals and grain-
810 size dependence of sediment composition. *Earth and Planetary Science Letters* 273,
811 138–151.

812 Gingeles, F., De Deckker, P., Norman, M., 2007. Late Pleistocene and Holocene climate of SE
813 Australia reconstructed from dust and river loads deposited offshore the River
814 Murray Mouth. *Earth and Planetary Science Letters* 255, 257–272.

815 Goldstein, S., Jacobsen, S.B., 1988. Nd and Sr isotopic systematics of river water suspended

816 material: implications for crustal evolution. *Earth and Planetary Science Letters* 87,
817 249–265.

818 Goldstein, S.L., Hemming, S.R., 2003. Long-lived isotopic tracers in oceanography,
819 paleoceanography, and ice-sheet dynamics. in *Treatise on Geochemistry: The Oceans*
820 *and Marine Geochemistry*, edited by H. D. Holland, et al., pp. 453-489, Elsevier.

821 Goldstein, S.L., O'niions, R.K., Hamilton, P.J., 1984. A Sm-Nd isotopic study of atmospheric
822 dusts and particulates from major river systems. *Earth and Planetary Science Letters*
823 70, 221–236.

824 Gourlan, A.T., Meynadier, L., Allègre, C.J., 2008. Tectonically driven changes in the Indian
825 Ocean circulation over the last 25 Ma: Neodymium isotope evidence. *Earth and*
826 *Planetary Science Letters* 267, 1-2, 353-364.

827 Götze, J., Lewis, R., 1994. Distribution of REE and trace elements in size and mineral
828 fractions of high-purity quartz sands. *Chemical Geology* 114, 43–57.

829 Haley, B.A., Frank, M., Spielhagen, R.F., Fietzke, J., 2008. Radiogenic isotope record of
830 Arctic Ocean circulation and weathering inputs of the past 15 million years.
831 *Paleoceanography* 23, PA1S13–.

832 Harris, N., Bickle, M., Chapman, H., Fairchild, I., Bunbury, J., 1998. The significance of
833 Himalayan rivers for silicate weathering rates: Evidence from the Bhote Kosi
834 tributary. *Chemical Geology* 144, 205–220.

835 Harrison, T.M., Blichert-Toft, J., Müller, W., Albarède, F., Holden, P., Mojzsis, S.J., 2005.
836 Heterogeneous Hadean Hafnium: Evidence of Continental Crust at 4.4 to 4.5 Ga.
837 *Science* 310, 1947–1950.

838 Hawkesworth, C.J., Dhuime, B., Pietranik, A.B., Cawood, P.A., Kemp, A.I.S., Storey, C.D.,
839 2010. The generation and evolution of the continental crust. *Journal of the Geological*
840 *Society* 167, 229–248.

841 Hawkesworth, C.J., Kemp, A., 2006. The differentiation and rates of generation of the
842 continental crust. *Chemical Geology* 226, 134–143.

843 Hu, B., Li, G., Li, J., Bi, J., Zhao, J., Bu, R., 2012. Provenance and climate change inferred from
844 Sr–Nd–Pb isotopes of late Quaternary sediments in the Huanghe (Yellow River) Delta,
845 China. *Quaternary Research* 78, 3, 561-571.

846 Innocent, C., Fagel, N., Stevenson, R.K., Hillaire-Marcel, C., 1997. Sm-Nd signature of
847 modern and late Quaternary sediments from the northwest North Atlantic:
848 Implications for deep current changes since the Last Glacial Maximum. *Earth and*
849 *Planetary Science Letters* 146, 607–625.

850 Johnson, M., Rogers, G., 1997. Rb-Sr ages of micas from the Kathmandu complex, Central
851 Nepalese Himalaya: Implications for the evolution of the Main Central Thrust. *Journal*
852 *of the Geological Society* 154, 863–869.

853 Kai, K., 1981. Rb-Sr Ages of the Biotite and Muscovite of the Himalayas, Eastern Nepal - Its
854 Implication in the Uplift History. *Geochem J* 15, 63–68.

855 Kamber, B.S., Greig, A., Collerson, K.D., 2005. A new estimate for the composition of
856 weathered young upper continental crust from alluvial sediments, Queensland,
857 Australia. *Geochimica et Cosmochimica Acta* 69, 1041–1058.

858 Kemp, A.I.S., Hawkesworth, C.J., Foster, G.L., Paterson, B.A., Woodhead, J.D., Hergt, J.M.,

859 Gray, C.M., Whitehouse, M.J., 2007. Magmatic and Crustal Differentiation History of
860 Granitic Rocks from Hf-O Isotopes in Zircon. *Science* 315, 980–983.

861 Komar, P.D., 2007. The Entrainment, Transport and Sorting of Heavy Minerals by Waves
862 and Currents, in: *Heavy Minerals in Use. Developments in Sedimentology*, pp. 3–48.

863 Le Fort, P., 1975. Himalayas: the collided range. Present knowledge of the continental arc.
864 *American Journal of Science* 275A, 1-44.

865 Lisitzin, A.P., 1996. *Oceanic Sedimentation: Lithology and Geochemistry*. American
866 Geophysical Union, Washington, D. C.

867 Lupker, M., France-Lanord, C., Galy, V., lavé, J., Gaillardet, J., Gajurel, A.P., Guilmette, C.,
868 Rahman, M., Singh, S.K., Sinha, R., 2012. Predominant floodplain over mountain
869 weathering of Himalayan sediments (Ganga basin). *Geochimica et Cosmochimica Acta*
870 84, 410-432.

871 Lupker, M., France-Lanord, C., lavé, J., Bouchez, J., Galy, V., Métivier, F., Gaillardet, J.,
872 Lartiges, B., Mugnier, J.-L., 2011. A Rouse-based method to integrate the chemical
873 composition of river sediments: Application to the Ganga basin. *J. Geophys. Res.* 116,
874 F04012.

875 McLennan, S.M., 1989. Rare earth elements in sedimentary rocks; influence of provenance
876 and sedimentary processes. *Reviews in mineralogy and geochemistry* 21, 169–200.

877 McLennan, S.M., 2001. Relationships between the trace element composition of
878 sedimentary rocks and upper continental crust. *Geochem. Geophys. Geosyst.* 2, 1021–
879 1024.

880 McLennan, S.M., McCulloch, M.T., Taylor, S.R., Maynard, J.B., 1989. Effects of sedimentary
881 sorting on neodymium isotopes in deep-sea turbidites. *Nature* 337, 547–549.

882 Mehta, P.K., 1977. Rb-Sr geochronology of the Kulu-Mandi Belt: Its implications for the
883 Himalayan Tectogenesis. *Int J Earth Sci (Geol Rundsch)* 66, 156–175.

884 Milliman, J., Meade, R.H., 1983. World-wide delivery of river sediment to the oceans. *The*
885 *Journal of Geology* 91, 1–21.

886 Millot, R., Allègre, C.J., Gaillardet, J., Roy, S., 2004. Lead isotopic systematics of major river
887 sediments: a new estimate of the Pb isotopic composition of the Upper Continental
888 Crust. *Chemical Geology* 203, 75–90.

889 Monecke, T., Bombach, G., Klemm, W., Kempe, U., Götze, J., Wolf, D., 2000. Determination
890 of trace elements in the quartz reference material UNS-SpS and in natural quartz
891 samples by ICP-MS. *Geostandards Newsletter* 24 (1), 73–81.

892 Padoan, M., Garzanti, E., Harlavan, Y., Villa, I.M., 2011. Tracing Nile sediment sources by Sr
893 and Nd isotope signatures (Uganda, Ethiopia, Sudan). *Geochimica et Cosmochimica*
894 *Acta* 75, 3627–3644.

895 Patchett, P.J., White, W.M., Feldmann, H., Kielinczuk, S., Hofmann, A.W., 1984.
896 Hafnium/rare earth element fractionation in the sedimentary system and crustal
897 recycling into the Earth's mantle. *Earth and Planetary Science Letters* 69, 365–378.

898 Pierson-Wickmann, A.C., Reisberg, L., France-Lanord, C., 2001. Os-Sr-Nd results from
899 sediments in the Bay of Bengal: Implications for sediment transport.
900 *Paleoceanography* 16, 435–444.

901 Piotrowski, A.M., Goldstein, S.L., Hemming, S.R., Fairbanks, R.G., 2004. Intensification and

902 variability of ocean thermohaline circulation through the last deglaciation. *Earth and*
903 *Planetary Science Letters* 225, 205–220.

904 Rahaman, W., Singh, S.K., Sinha, R., Tandon, S.K., 2009. Climate control on erosion
905 distribution over the Himalaya during the past 100 ka. *Geology* 37, 559–562.

906 Revel, M., Cremer, M., Grousset, F.E., Labeyrie, L., 1996. Grain-size and Sr-Nd isotopes as
907 tracer of paleo-bottom current strength, Northeast Atlantic Ocean. *Marine Geology*
908 131, 233–249.

909 Richards, A., Argles, T., Harris, N., Parrish, R., Ahmad, T., Darbyshire, F., Draganits, E., 2005.
910 Himalayan architecture constrained by isotopic tracers from clastic sediments. *Earth*
911 *and Planetary Science Letters* 236, 773–796.

912 Roddaz, M., Viers, J., Brusset, S., Baby, P., Hérail, G., 2005. Sediment provenances and
913 drainage evolution of the Neogene Amazonian foreland basin. *Earth and Planetary*
914 *Science Letters* 239, 57–78.

915 Rudnick R L and Gao S. 2003. Composition of the Continental Crust. pp 1–64. In *The Crust*
916 (ed. R.L. Rudnick) Vol. 3, *Treatise on Geochemistry* (eds. H.D. Holland and K.K.
917 Turekian), Elsevier-Pergamon, Oxford.

918 Singh, S.K., France-Lanord, C., 2002. Tracing the distribution of erosion in the
919 Brahmaputra watershed from isotopic compositions of stream sediments. *Earth and*
920 *Planetary Science Letters* 202, 645–662.

921 Singh, S.K., Rai, S.K., Krishnaswami, S., 2008. Sr and Nd isotopes in river sediments from
922 the Ganga Basin: Sediment provenance and spatial variability in physical erosion. *J.*
923 *Geophys. Res.* 113, F03006.

924 Stille, P., Steinmann, M., Riggs, S.R., 1997. Nd isotope evidence for the evolution of the
925 paleocurrents in the Atlantic and Tethys oceans during the past 180 Ma. *Oceanographic Literature Review* 44, 698–698.

926 Stummeyer, J., Marchig, V., Knabe, W., 2002. The composition of suspended matter from
927 Ganges–Brahmaputra sediment dispersal system during low sediment transport
928 season. *Chemical Geology* 185, 125–147.

929 Stumpf, R., Frank, M., Schönfeld, J., Haley, B.A., 2011. Climatically driven changes in
930 sediment supply on the SW Iberian shelf since the Last Glacial Maximum. *Earth and*
931 *Planetary Science Letters* 312, 80–90.

932 Taylor, S.R., McLennan, S.M., 1995. The Geochemical evolution of the Continental Crust.
933 *Reviews of Geophysics* 33, 241–265.

934 Veevers, J.J., Saeed, A., Belousova, E.A., Griffin, W., 2005. U-Pb ages and source composition
935 by Hf-isotope and trace-element analysis of detrital zircons in Permian sandstone and
936 modern sand from southwestern Australia and a review of the paleogeographical and
937 denudational history of the Yilgam Craton. *Earth Science Reviews* 68, 245–279.

938 Vervoort, J., Plank, T., Prytulak, J., 2011. The Hf-Nd isotopic composition of marine
939 sediments. *Geochimica et Cosmochimica Acta* 75, 5903–5926.

940 Vervoort, J.D., Patchett, P.D., Blichert-Toft, J., Albarède, F., 1999. Relationships between
941 Lu–Hf and Sm–Nd isotopic systems in the global sedimentary system. *Earth and*
942 *Planetary Science Letters* 168, 79–99.

943 Walter, H.J., Hegner, E., Diekmann, B., Kuhn, G., 2000. Provenance and transport of
944

- 945 terrigenous sediment in the South Atlantic Ocean and their relations to glacial and
946 interglacial cycles: Nd and Sr isotopic evidence. *Geochimica et Cosmochimica Acta* 64,
947 3813–3827.
- 948 Wu, W., Xu, S., Yang, J., Yin, H., Lu, H., Zhang, K., 2010. Isotopic characteristics of river
949 sediments on the Tibetan Plateau. *Chemical Geology* 269, 406–413.
- 950 Yan, Y.L., Xia, B., Lin, G.E., Carter, A., Hu, X., Cui, X., Liu, B., Yan, P., Song, Z., 2007.
951 Geochemical and Nd isotope composition of detrital sediments on the north margin
952 of the South China Sea: provenance and tectonic implications. *Sedimentology* 54, 1–
953 17.
- 954 Zeh, A., Gerdes, A., Klemd, R., Barton, J.M., 2007. Archaean to Proterozoic Crustal Evolution
955 in the Central Zone of the Limpopo Belt (South Africa-Botswana): Constraints from
956 Combined U-Pb and Lu-Hf Isotope Analyses of Zircon. *Journal of Petrology* 48, 1605–
957 1639.
- 958

959 **Tables**

960 **Table 1:** Trace element concentrations (ppm) and Nd-Hf-Sr-Pb isotopes of the mineral
961 fractions separated from the Ganga sediments.

962 *Footnotes:* * Data already published by Garçon et al. (2013b). $\pm 2\sigma$ are in-run errors.

963

Table 1: Trace element concentrations (ppm) and Nd-Hf-Sr-Pb isotopic compositions of the mineral fractions separated from the Ganga sediments.

Sample Name	BR 717 Msc	BR 717 Bio	BR 717 Fd-K	BR 717 Fd-K Dup	BR 717 Pig	BR 717 Qtz	BR 717 Mag	BR 717 Ep	BR 717 Grt	BR 717 Tn	BR 717 Amp	BR 717 Carb	BR 717 Zrn	BR 717 Mnz	BR 717 Ap	BGP 6 A
Type of mineral	Muscovite	Biotite	K-Feldspar	K-Feldspar (Duplicate)	Plagioclase	Quartz	Magnetite	Epidote	Garnet	Titanite	Amphibole	Carbonate	Zircon	Rich in Monazite and Allanite	Rich in Apatite	Clay
Cs	15.4	65.9	8.94		0.838	0.209	0.579	0.267	0.153	0.557	1.80	0.00913	0.214	0.935	0.504	17.0
Rb	311	435	313		31.1	3.34	7.37	2.54	1.50	9.73	23.3	0.846	3.03	12.0	9.16	167
Ba	967	478	1393		146	19.8	33.0	14.9	3.49	39.9	60.2	16.6	7.01	71.3	427	373
Th	4.58	24.9	4.10		2.37	2.91	13.7	17.8	15.6	151	24.0	1.17	219	2374	28.8	62.0
U	1.54	2.36	0.663		0.622	0.83	3.61	6.49	3.49	50.1	7.40	0.522	612	400	28.9	8.55
Nb	36.1	87.3	0.992		1.39	0.581	20.8	3.69	3.25	229	403	< DL	171	1068	119	16.7
Ta	2.78	9.58	0.112		0.106	0.0304	1.66	0.267	0.42	31.0	43.5	0.013	17.9	162	8.24	1.49
La	9.99	60.9	4.41		3.74	5.23	19.8	62.2	172	172	32.6	6.89	32.8	3763	71.1	1021
Ce	27.5	110	14.3		14.4	11.3	41.1	134	91.0	527	71.6	14.7	113	7785	206	206
Pr	2.34	18.2	1.07		0.933	1.29	4.58	17.2	9.79	93.1	8.76	1.95	16.3	883	30.3	24.3
Pb	11.1	4.96	75.1		12.6	3.89	19.1	46.9	0.916	5.52	24.1	7.28	19.3	81.9	7.98	95.2
Nd	8.29	32.0	3.77		3.57	4.59	16.6	71.8	34.5	414	34.1	8.25	79.6	3180	146	90.5
Sr	32.3	7.01	243		195	70.6	11.8	1509	3.31	52.9	38.4	5.26	16.9	274	197	47.9
Sm	1.57	4.77	0.837		0.684	1.04	3.17	17.6	7.83	105	7.88	2.07	32.7	670	54.0	17.3
Zr	210	264	21.9		94.4	27.1	265	183	251	2128	539	< DL	416415	20849	4240	447
Hf	5.70	7.30	0.658		2.56	0.749	7.01	4.76	6.95	72.8	15.5	< DL	10171	639	119	12.2
Ti	4898	16573	185		273	71.4	17180	2706	770	32279	168099	2.29	41321	107327	18799	6416
Eu	0.253	0.416	0.744		0.30	0.176	0.54	5.75	1.01	19.4	1.73	0.523	7.19	59.8	6.20	2.70
Gd	1.25	3.41	0.733		0.585	0.921	2.74	18.2	16.4	100	8.96	2.37	65.1	494	74.3	14.3
Tb	0.185	0.462	0.118		0.0907	0.155	0.46	2.94	5.95	17.4	1.78	0.414	17.8	61.5	14.1	2.02
Dy	1.14	2.59	0.658		0.537	1.01	2.86	18.6	60.9	113	13.3	2.59	178	310	88.5	11.4
Ho	0.226	0.474	0.127		0.108	0.214	0.612	3.78	15.7	22.0	2.83	0.577	55.7	52.5	16.2	2.12
Y	6.49	13.6	3.77		3.39	6.65	17.0	110	379	536	86.1	19.4	1463	1148	432	58.0
Er	0.677	1.32	0.345		0.335	0.645	1.83	10.6	52.0	62.7	8.42	1.76	243	140	42.3	5.84
Lu	24.6	394	11.8		0.461	5.96	3.69	3.42	14.3	8.78	26.2	0.889	15.7	19.8	13.3	40.8
Yb	0.685	1.22	0.322		0.381	0.587	1.92	9.61	58.0	58.9	8.50	1.82	424	140	33.3	5.21
Re-run	0.198	0.192	0.0478		0.062	0.0861	0.296	1.39	8.54	7.91	1.22	0.283	83.5	21.3	4.47	0.738
Sc	13.3	27.3	0.655		0.917	8.14	90.1	102	33.8	45.8	32.5	1.95	325	251	32.0	19.7
V	171	243	1.89		6.86	8.08	1281	414	54.4	139	943	< DL	99.2	408	128	220
Cr	91.3	144	2.74		5.13	3.34	1950	131	76.1	44.8	197	2.00	70.7	236	81.1	143
Co	2.76	47.9	0.691		0.907	0.269	51.0	2.69	23.8	0.683	44.6	0.956	0.443	2.83	1.25	27.3
Ni	6.39	79.7	2.77		3.62	0.464	170	6.34	1.55	3.28	35.6	1.40	3.86	4.74	2.50	99.0
¹⁴³ Nd/ ¹⁴⁴ Nd ± 2σ	0.511844 ± 15	0.511834 ± 11	0.511834 ± 19		0.511901 ± 33		0.512089 ± 9	0.512235 ± 10	0.511906 ± 11	0.512182 ± 9	0.511929 ± 24	0.511843 ± 10	0.512062 ± 10	0.511732 ± 8	0.511921 ± 7	0.511827 ± 10
Re-run					0.511820 ± 9									0.511741 ± 6		
¹⁷⁶ Hf/ ¹⁷⁷ Hf ± 2σ	0.282218 ± 9	0.282162 ± 11	0.282400 ± 15	0.282313 ± 15	0.282325 ± 9		0.282602 ± 8	0.282803 ± 12	0.282698 ± 5	0.282955 ± 16	0.282236 ± 8		0.281970 ± 5		0.282234 ± 8	
⁸⁷ Sr/ ⁸⁶ Sr ± 2σ	0.831306 ± 10	0.812332 ± 8	0.758656 ± 8	0.755512 ± 7	0.722744 ± 8		0.728827 ± 7	0.712509 ± 7	0.746224 ± 8	0.722704 ± 7	0.725748 ± 8	0.713942 ± 8	0.734440 ± 20		0.746642 ± 8	
²⁰⁸ Pb/ ²⁰⁶ Pb ± 2σ *	20.2008 ± 16	20.5508 ± 26	19.3257 ± 16	19.3318 ± 12	18.9724 ± 18		19.5343 ± 14	18.9028 ± 14		31.4562 ± 22	19.9482 ± 12	19.9809 ± 8			18.8658 ± 12	

964 **Table 2:** Sr isotopic compositions of bedloads and suspended loads sampled at the
965 outflow of the Ganga River.

966 *Footnotes:* * These Sr isotopic compositions were analyzed on the silicate fractions of the
967 sediments (i.e. after a leaching in 1N acetic acid) in Nancy, France, following the methods
968 described by Galy et al. (1999). DL stands for detection limit. $\pm 2\sigma$ are in-run errors.

969

970

Table 2: Sr isotopes in bedloads and suspended loads sampled at the outflow of the Ganga River

Sample Name	Latitude	Longitude	Sampling date	Type of sediment	Sampling depth (m)	$^{86}\text{Sr}/^{87}\text{Sr}$	$\pm 2\sigma$	Percentage of the bulk sample (%)	Sr (ppm)
BGP 6	24.35833	88.60833	2-Aug-93	Bedload		0.758885	8		115
BR 414	24.05290	89.02465	13-Jul-04	Suspended Load	2	0.773743	8		91.0
BR 412	24.05290	89.02465	13-Jul-04	Suspended Load	6.5	0.768185	12		101
BR 418	24.05290	89.02465	13-Jul-04	Bedload	10	0.754593	8		103
BR 717	24.05290	89.02465	17-Aug-07	Bedload	11	0.757160	8		98.3
BR 522*	24.04187	89.0362	23-Jul-05	Suspended load	0	0.771110	10		95.8
BR 522 50-200 μm^*								4.6	98.3
BR 522 20-50 μm^*						0.755340	10	42.8	99.3
BR 522 2-20 μm^*						0.782400	10	42.2	83.0
BR 522 0.2-2 μm^*						0.757570	10	10.3	48.4

971 **Figures**

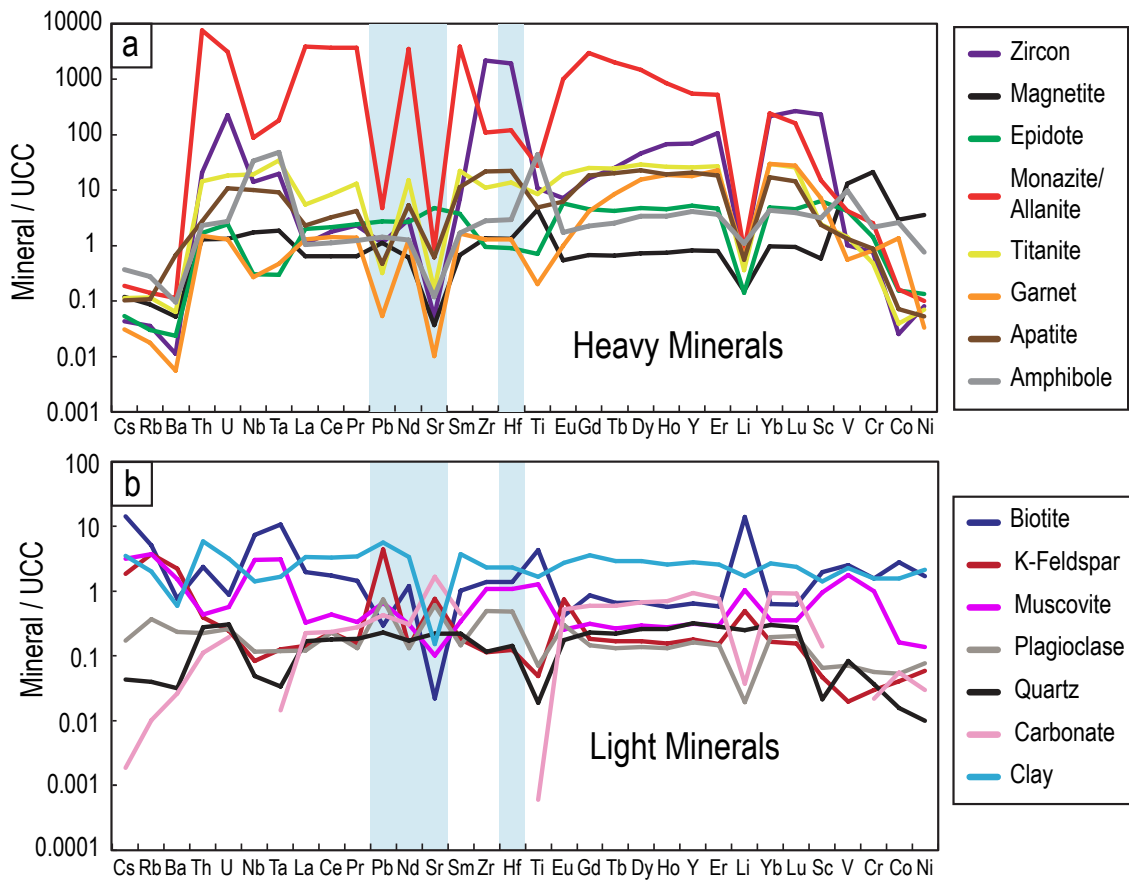
972 **Figure 1:** Map of the Bangladesh delta showing sampling sites for river sediments.

973 **Figure 1**



986 **Figure 2:** Trace element patterns normalized to the average composition of the upper
 987 continental crust (UCC) of Rudnick and Gao (2003). **a)** Heavy minerals. **b)** Light minerals
 988
 989

Figure 2



990 **Figure 3:** Results of the Monte-Carlo simulation for Nd isotopes.

991 Proportions of minerals used to perform the Monte-Carlo simulation are shown in the

992 histogram in the top right corner of the Figure (see Supplementary File for more details).

993 Color dots indicate the contributions of the different minerals to the Nd isotopic

994 compositions of the 100,000 modeled mixtures. The contributions of carbonate, garnet,

995 amphibole, epidote, apatite, zircon, magnetite, muscovite, plagioclase, and K-feldspar are

996 not shown in this figure because they represent less than 10% of the whole range of

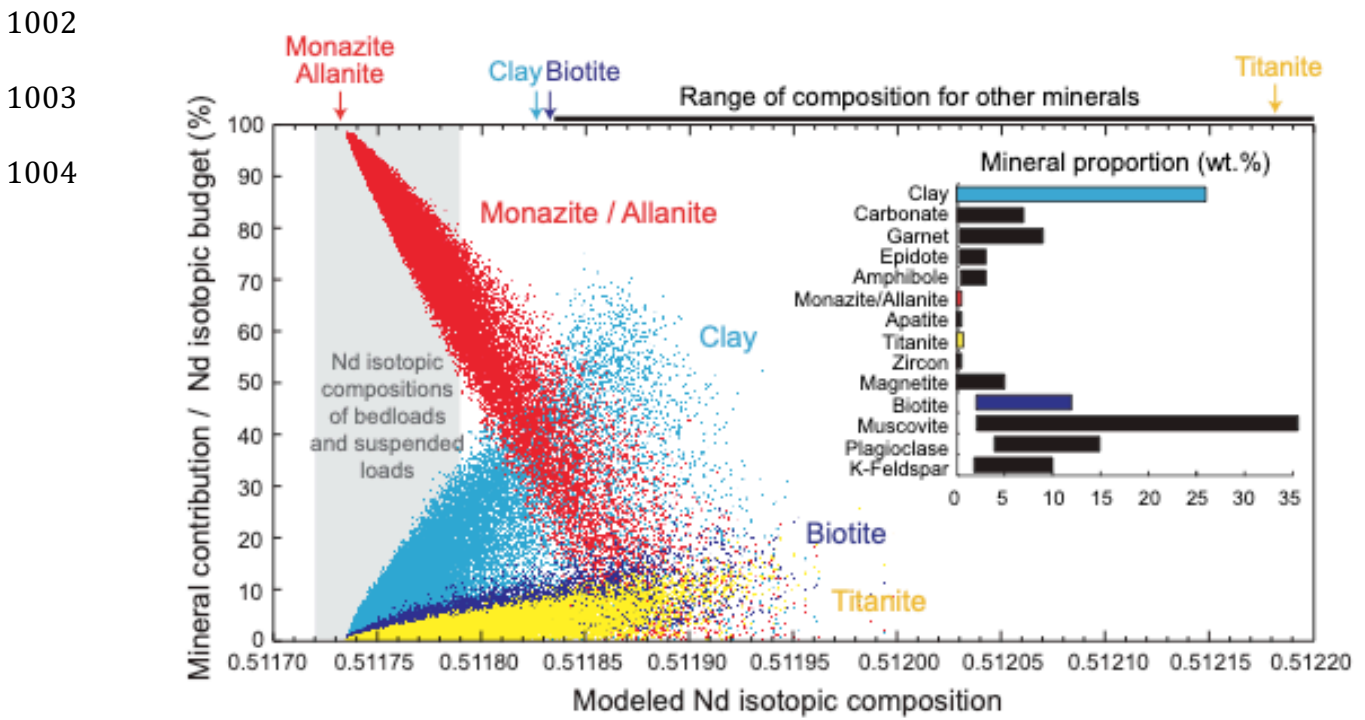
997 modeled Nd isotopic compositions. The vertical light grey band shows the range of Nd

998 isotopic compositions measured in bedloads and suspended loads sampled at the outflow

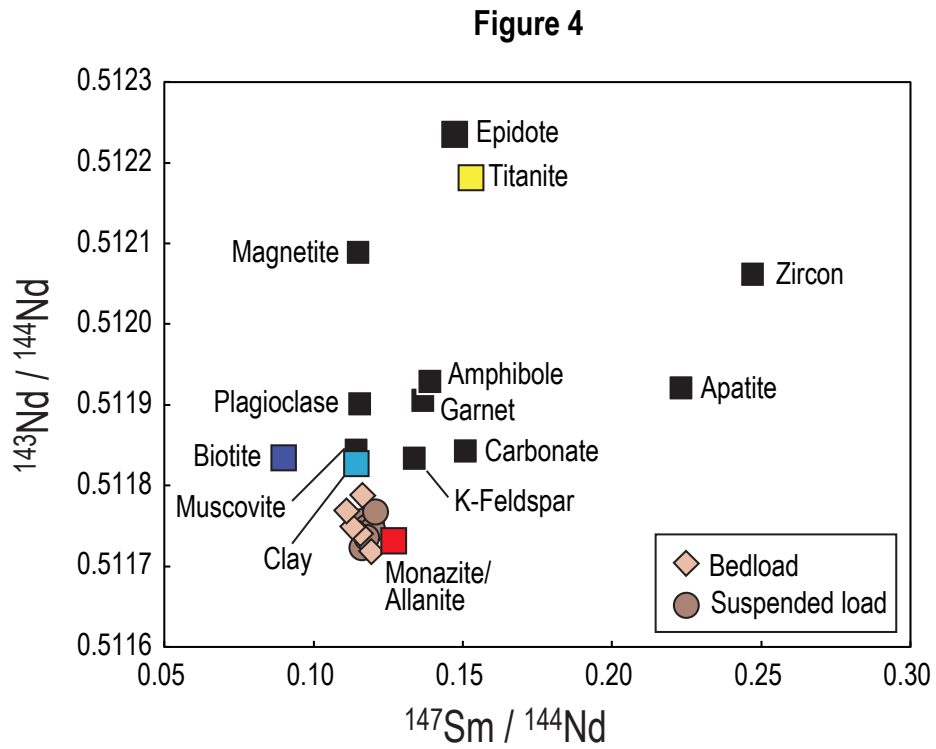
999 of the Ganga River and was constructed using the data of Garçon et al. (2013a). Arrows

1000 on the top axis indicate isotopic compositions of the most important minerals while the

1001 black line shows the range of isotopic compositions for all other minerals.



1005 **Figure 4:** Variations of $^{143}\text{Nd}/^{144}\text{Nd}$ ratios against $^{147}\text{Sm}/^{144}\text{Nd}$ ratios for the different
 1006 mineral fractions.
 1007 Bedloads and suspended loads shown in this Figure were sampled at the outflow of the
 1008 Ganga River. Data are from Garçon et al. (2013a).



1009
 1010
 1011
 1012
 1013
 1014
 1015
 1016
 1017
 1018
 1019

1020 **Figure 5:** Results of the Monte-carlo simulation for Hf isotopes.

1021 Proportions of minerals used to perform the Monte-Carlo simulation are shown in the

1022 histogram in the top right corner of the Figure (see Supplementary File for more details).

1023 Color dots indicate the contributions of the different minerals to the Hf isotopic

1024 compositions of the 100,000 modeled mixtures. The contributions of garnet, epidote,

1025 magnetite, amphibole, plagioclase, and K-feldspar are not shown in this figure because

1026 they represent less than 10% of the whole range of modeled Hf isotopic compositions.

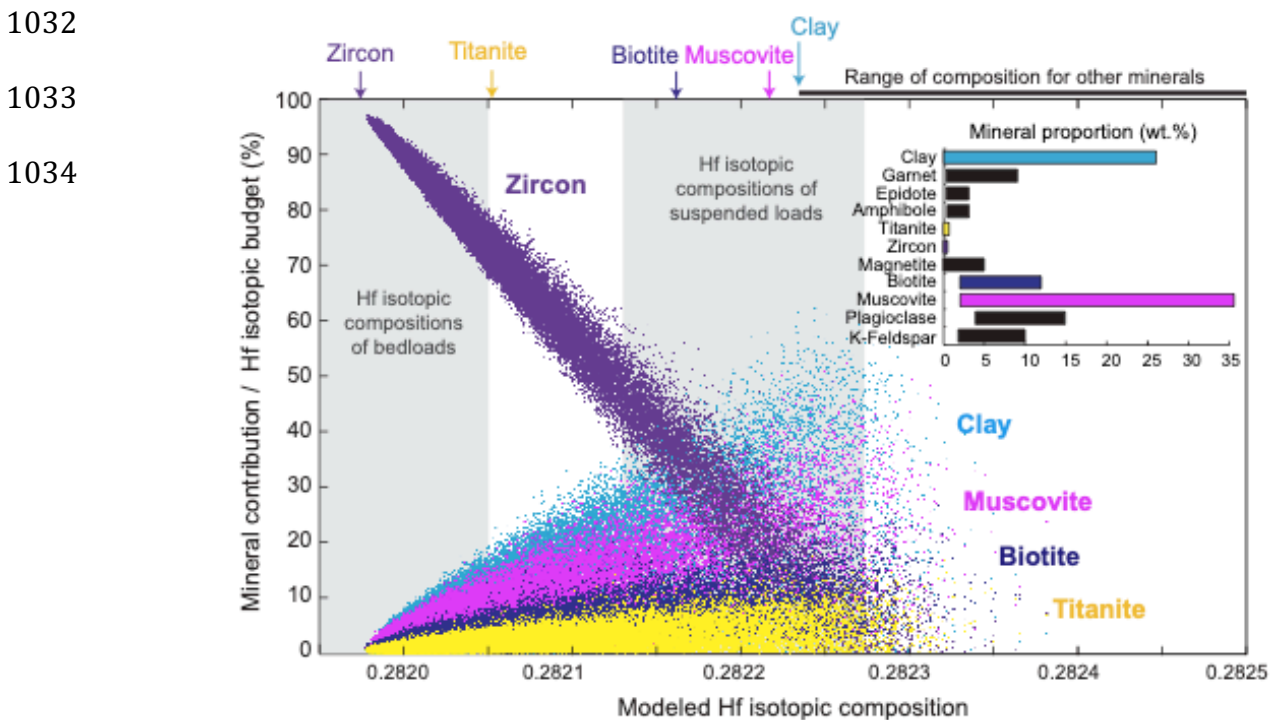
1027 Vertical light grey bands show the range of Hf isotopic compositions measured in

1028 bedloads and suspended loads sampled at the outflow of the Ganga River and were

1029 constructed using the data of Garçon et al. (2013a). Arrows on the top axis indicate

1030 isotopic compositions of the most important minerals while the black line shows the

1031 range of isotopic compositions for all other minerals.



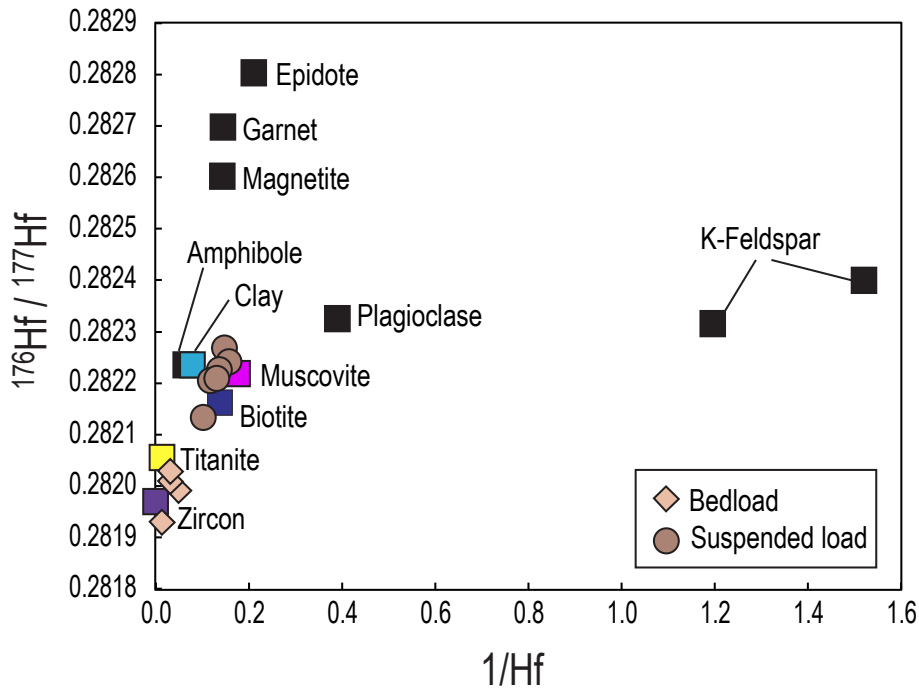
1035 **Figure 6:** Variations of $^{176}\text{Hf}/^{177}\text{Hf}$ ratios against $1/\text{Hf}$ ratios for the different mineral
1036 fractions.

1037 Data for bedloads and suspended loads sampled at the outflow of the Ganga River are
1038 from Garçon et al. (2013a). $1/\text{Hf}$ ratios of river sediments have been recalculated on a
1039 quartz-free basis by normalizing their SiO_2 contents, as published by Lupker et al. (2011),
1040 to that of our clay fraction (i.e. 43 wt%). Normalized $1/\text{Hf}$ ratios were thus calculated
1041 following this equation: $(1/\text{Hf})_N = (1/\text{Hf})_{\text{sample}} * (\text{SiO}_2, \text{clay} / \text{SiO}_2, \text{sample})$

1042

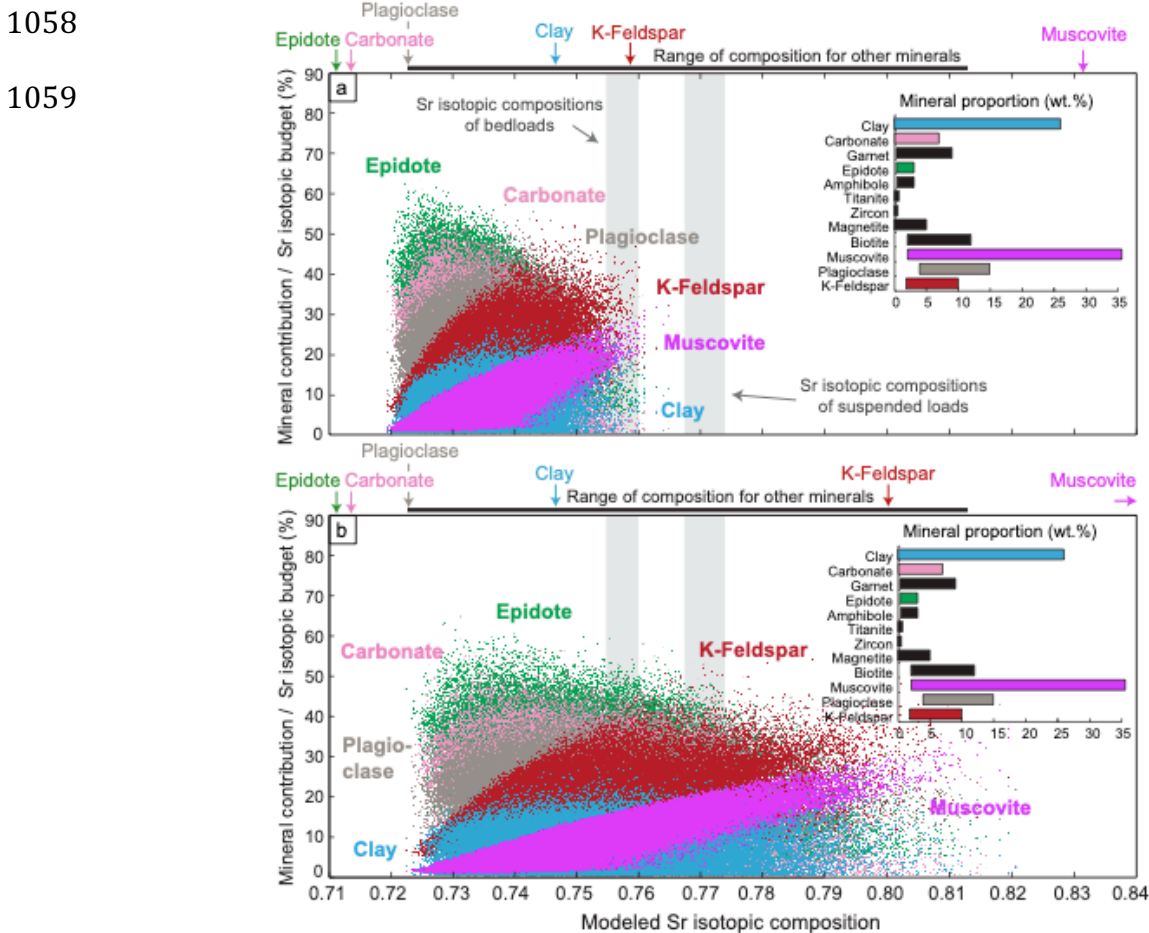
1043

Figure 6



1044 **Figure 7:** Results of the Monte-Carlo simulation for Sr isotopes.

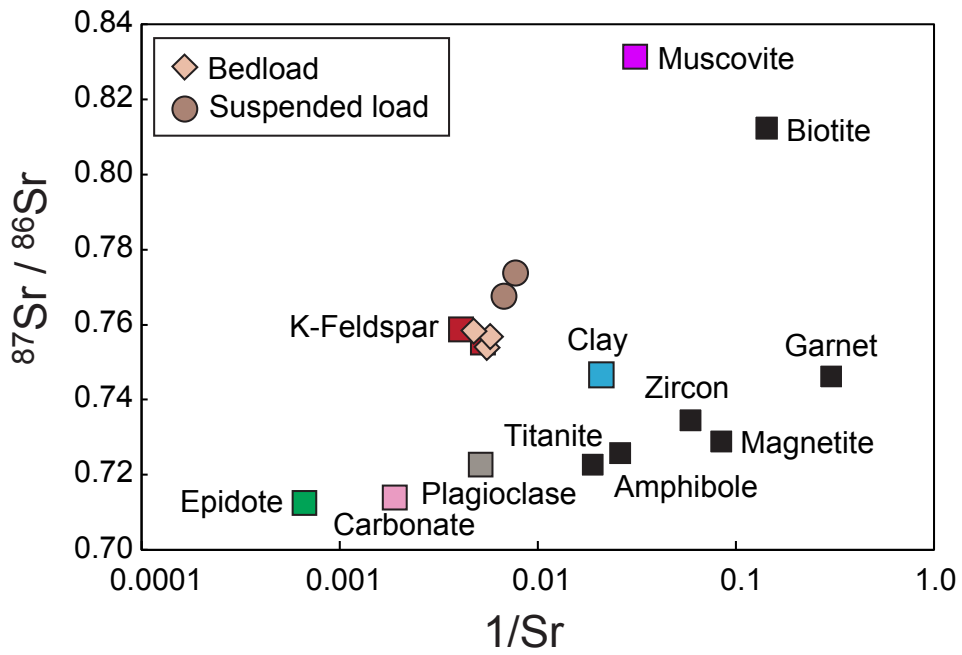
1045 **a)** Monte-Carlo simulation performed using the Sr isotopic compositions as measured in
1046 our mineral fractions. **b)** Monte-Carlo simulation performed using an $^{87}\text{Sr}/^{86}\text{Sr}$ ratio of
1047 0.800 for the K-feldspar fraction and 1.000 for the muscovite fraction. Proportions of
1048 minerals used to perform the Monte-Carlo simulation are shown in the histograms in the
1049 top right corner of the Figures (see Supplementary File for more details). Color dots
1050 indicate the contributions of the different minerals to the Sr isotopic compositions of the
1051 100,000 modeled mixtures. The contributions of garnet, amphibole, titanite, zircon,
1052 magnetite, and biotite are not shown in this figure because they represent less than 10%
1053 of the whole range of modeled Sr isotopic compositions. Vertical light grey bands show
1054 the range of Sr isotopic compositions measured in bedloads and suspended loads sampled
1055 at the outflow of the Ganga River and analyzed in this study. For each simulation, arrows
1056 on the top axis indicate isotopic compositions of the most important minerals while the
1057 black line shows the range of isotopic compositions for all other minerals.



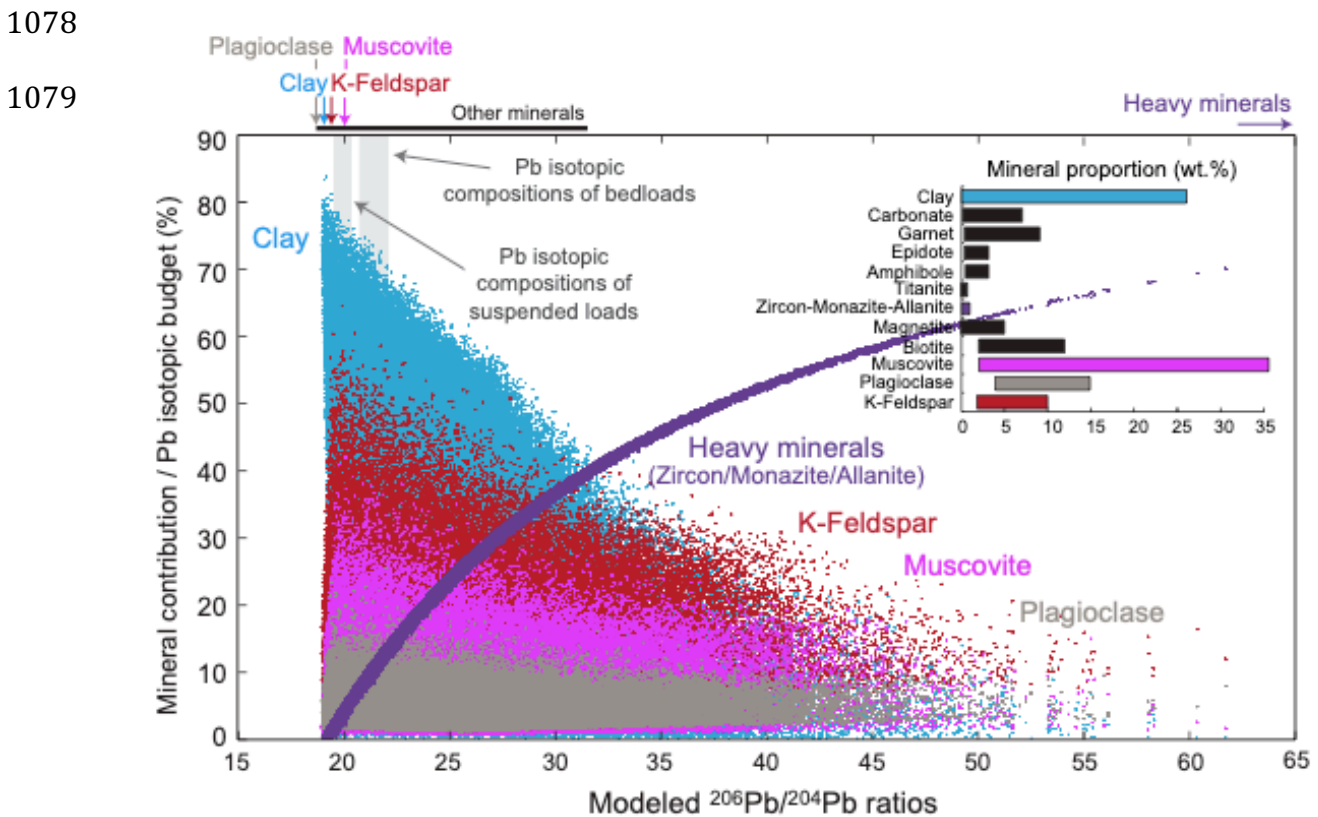
1060 **Figure 8:** Variations of $^{87}\text{Sr}/^{86}\text{Sr}$ ratios against $1/\text{Sr}$ ratios (logarithmic scale) for the
1061 different mineral fractions and the river sediments analyzed in this study. As in Figure 6,
1062 we normalized the $1/\text{Sr}$ ratios of bedloads and suspended loads using their SiO_2 contents
1063 and that of the clay fraction to correct from quartz dilution effects.

1064

1065



1066 **Figure 9:** Results of the Monte-Carlo simulation for Pb isotopes.
 1067 Proportions of minerals used to perform the Monte-Carlo simulation are shown in the
 1068 histograms in the top right corner of the Figures (see Supplementary File for more
 1069 details). Color dots indicate the contributions of the different minerals to the Pb isotopic
 1070 compositions of the 100,000 modeled mixtures. The contributions of carbonate, garnet,
 1071 epidote, amphibole, titanite, magnetite and biotite are not shown in this figure because
 1072 they represent less than 10% of the whole range of modeled $^{206}\text{Pb}/^{204}\text{Pb}$ ratios. Vertical
 1073 light grey bands show the range of Pb isotopic compositions measured in bedloads and
 1074 suspended loads sampled at the outflow of the Ganga River and were constructed using
 1075 the data of Garçon et al. (2013b). Arrows on the top axis indicate isotopic compositions of
 1076 the most important minerals while the black line shows the range of isotopic
 1077 compositions for all other minerals.



Supplementary File

Input parameters for the Monte-Carlo simulations

- **Mineral proportions**

Based on the mineral proportions estimated in suspended loads and bedloads by Garzanti et al. (2010, 2011) and Lupker et al. (2012) (see Supplementary Table 1), we defined possible ranges of weight proportions for the most important mineral species in the Ganga river sediments (see Table A below). We combined the albite and Ca-plagioclase estimates from Garzanti et al. (2010; 2011) to determine a range for plagioclase; similarly, we combined the calcite + dolomite estimates from Garzanti et al. (2010; 2011) and Lupker et al. (2012) to estimate the carbonate proportion and we used the opaques + Fe-oxides estimates from Garzanti et al. (2010; 2011) to establish the proportion of magnetite. The first column of Table A shows the range of proportions used for the simulations that are shown in Figures 3, 5, 7 and 9. We deliberately choose to use ranges that are larger than those determined by Garzanti et al (2010, 2011) and Lupker et al. (2012) to insure that our simulations maximize the errors and include extreme scenarios. The second column in Table A provides the ranges used to assess the robustness of the method (see below).

	Range of proportions used for the simulations	Range of proportions used to assess the robustness of the simulations
K-feldspar	2 – 10 wt.%	0 – 20 wt.%
Plagioclase (albite + Ca-plagioclase)	4 – 15 wt.%	0 – 30 wt.%
Muscovite	2 – 36 wt.%	0 – 72 wt.%
Biotite	2 – 12 wt.%	0 – 24 wt.%
Magnetite (opaques + Fe-oxides)	0 – 5 wt.%	0 – 10 wt.%
Zircon	0 – 0.5 wt.%	0 – 1 wt.%
Titanite	0 – 0.7 wt.%	0 – 1.4 wt.%
Apatite	0 – 0.5 wt.%	0 – 1 wt.%
Monazite/Allanite	0 – 0.5 wt.%	0 – 1 wt.%
Amphibole	0.3 – 3.0 wt.%	0 – 6 wt.%
Epidote	0.2 – 3.0 wt.%	0 – 6 wt.%
Garnet	0.2 – 9.0 wt.%	0 – 18 wt.%
Carbonate (calcite + dolomite)	0.5 – 7 wt.%	0 – 14 wt.%
Clay	0 – 26 wt.%	0 – 52 wt.%

Table A: Ranges of mineral proportions used for the Monte-Carlo simulations

Some of the minerals identified by Garzanti et al. (2010, 2011) (Supplementary Table 1) are not included in our simulations: quartz, chlorite, tourmaline, rutile, Ti oxide, pyroxene, spinel, chloritoid, staurolite, kyanite, sillimanite, fibrolite, olivine and xenotime. Garzanti et al. (2010, 2011) showed that these minerals contribute to less than 2% in the Nd, Hf, Sr and Pb elemental budgets of the sediments. We therefore chose to minimize the analytical work and did not analyze their trace element contents and isotopic compositions.

- **Concentrations and isotopic compositions of minerals**

We performed the Monte-Carlo simulations using the Nd, Hf, Sr, Pb concentrations and isotopic compositions of mineral separates as listed in Table 1. The only exceptions are the Nd concentrations of monazite and apatite that we took from Garzanti et al. (2010, 2011) (94, 000 ppm and 635 ppm, respectively) because the fractions that we analyzed were not pure enough. In the fraction that we measured, the REE are certainly diluted by the presence of other minerals but we are still confident that the Nd isotopic compositions are representative of the pure minerals. As explained in the main text of the manuscript, only one analysis was performed for each mineral species because of the complexity of the mineral separation procedure and the limited amount of samples available for the study. However, a large number of grains were analyzed in each mineral fraction, meaning that our measurements should be representative of the average compositions of the mineral populations. Errors in the simulations associated to such uncertainties are evaluated below.

Monte-Carlo simulations

For each mineral species, proportions were randomly sampled ($n=100,000$) in uniform distributions within the range of proportions indicated in the Table A (first column). The simulations were designed to allow the sum of the mineral proportions to add up to more or less than 100% because the calculations done in the simulations use relative mineral proportions only, hence this does not influence the final results. We have tested other simulations in which the mineral proportions were rejected and re-sampled if their sums were $>105\%$ and/or $<95\%$ but this does not change the results of the simulations. Then, using these proportions together with concentrations and isotopic compositions of individual minerals, we calculated the isotopic compositions of the resulting mixtures.

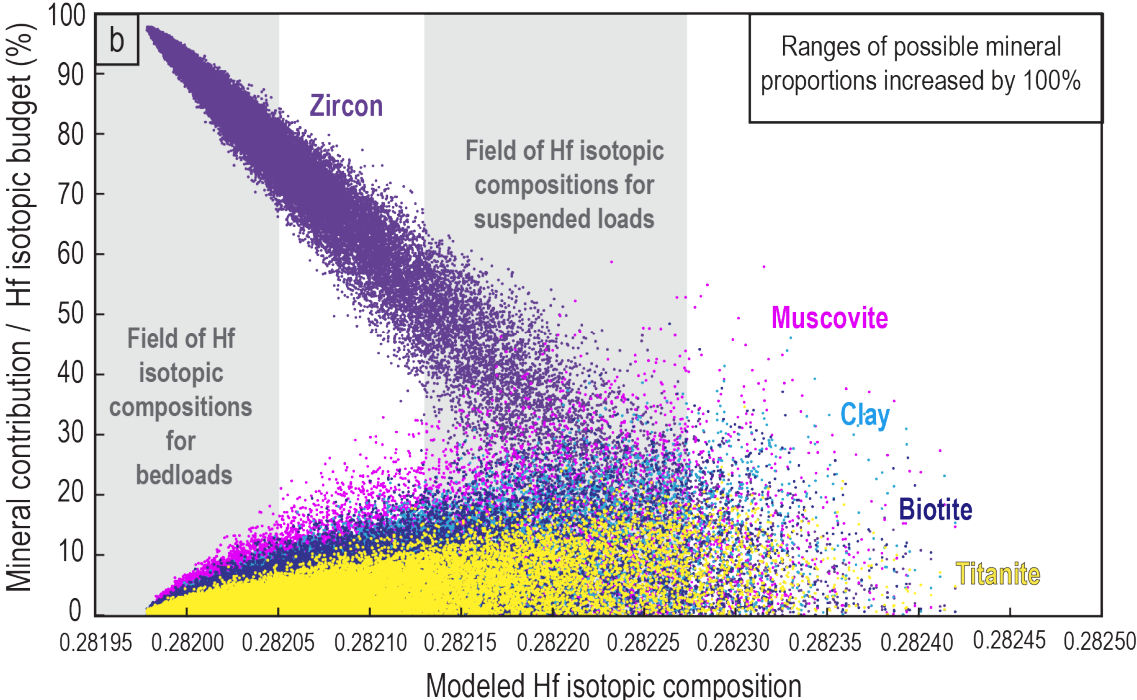
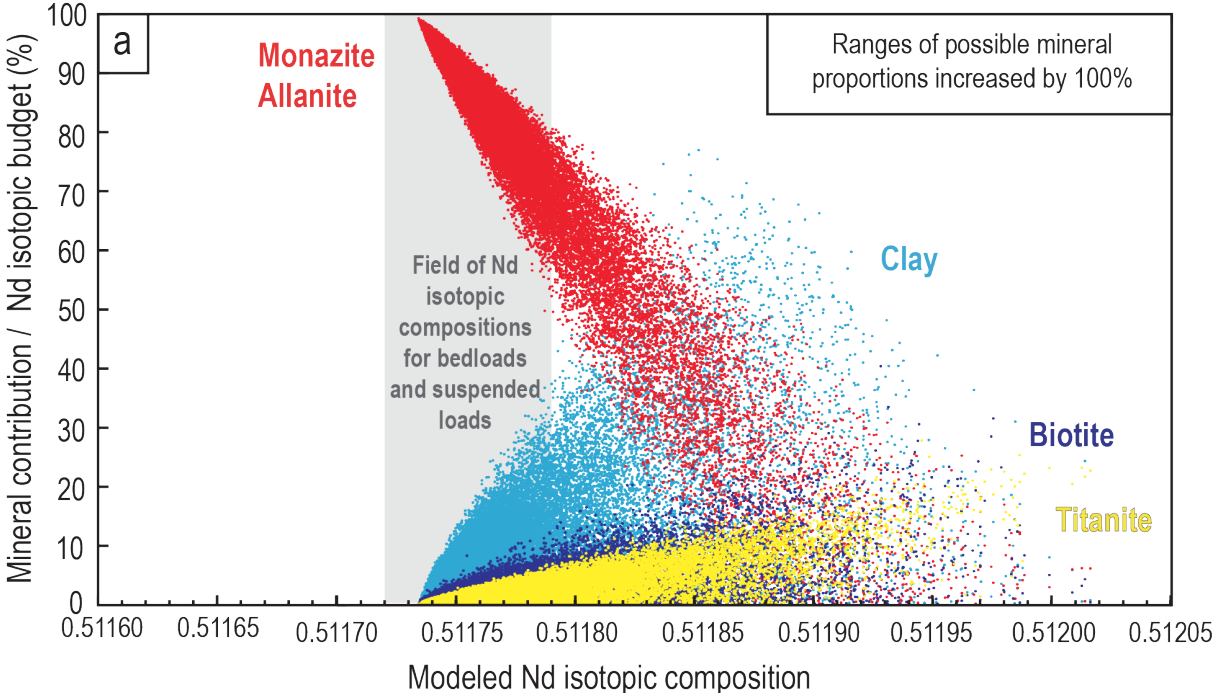
Note that Nd, Hf, Pb and Sr concentrations modeled by this set of Monte-Carlo simulations are not identical to concentrations measured in sediments because (a) the percentages of important minerals are relative and not absolute, and (b) we did not take into account quartz that significantly dilutes all concentrations. This is why we performed other simulations not shown here. They were designed to model only the concentrations in the sediments but not the isotopic compositions. Results showed that the range of Nd, Hf, Sr and Pb concentrations in the Ganga sediments are perfectly reproduced when quartz is added to the minerals listed in Table A.

Robustness of the Monte-Carlo simulations

To assess the robustness and uncertainties of the Monte-Carlo simulations we performed several tests. We first increased the ranges of possible mineral proportions by 100% (second column in Table A) to evaluate the sensitivity of the simulations to this parameter. Results are shown below in Figure A for the four isotopic systems. The important point is that the contribution of the different mineral species to the isotopic budgets of the Himalayan sediments remain remarkably similar, showing that the simulation results are well constrained. The mineralogy would need to be completely different for the results to be modified. In turn, this implies that the results presented in this study should be valid for most sediment sampled in large river systems all over the world.

We also tested the sensitivity of the simulations to changes of both concentrations and isotopic compositions of the minerals. To do that, we added an initial step that randomly samples the concentrations and isotopic compositions of each mineral species in given Gaussian distributions centered on the values that we measured in the mineral separates. We deliberately assumed very large errors on the values, with standard deviations (2σ) of $\pm 20\%$ for the concentrations, ± 0.0001 for Nd and

Hf isotopic compositions, ± 0.01 for Sr isotopic compositions and $\pm 1\%$ for Pb isotopic compositions. The rest of the calculation is similar to those shown in Figures 3, 5, 7 and 8. The results of these simulations (not shown here) indicate that the contributions of the different mineral species to the isotopic budget of the Ganga sediments still remain the same as in Figures 3, 5, 7 and 8. The uncertainties entailed by our data set are thus limited and we are confident that the results presented in this study would not significantly change even if our data set did not catch all the compositional heterogeneity of the Himalayan minerals.



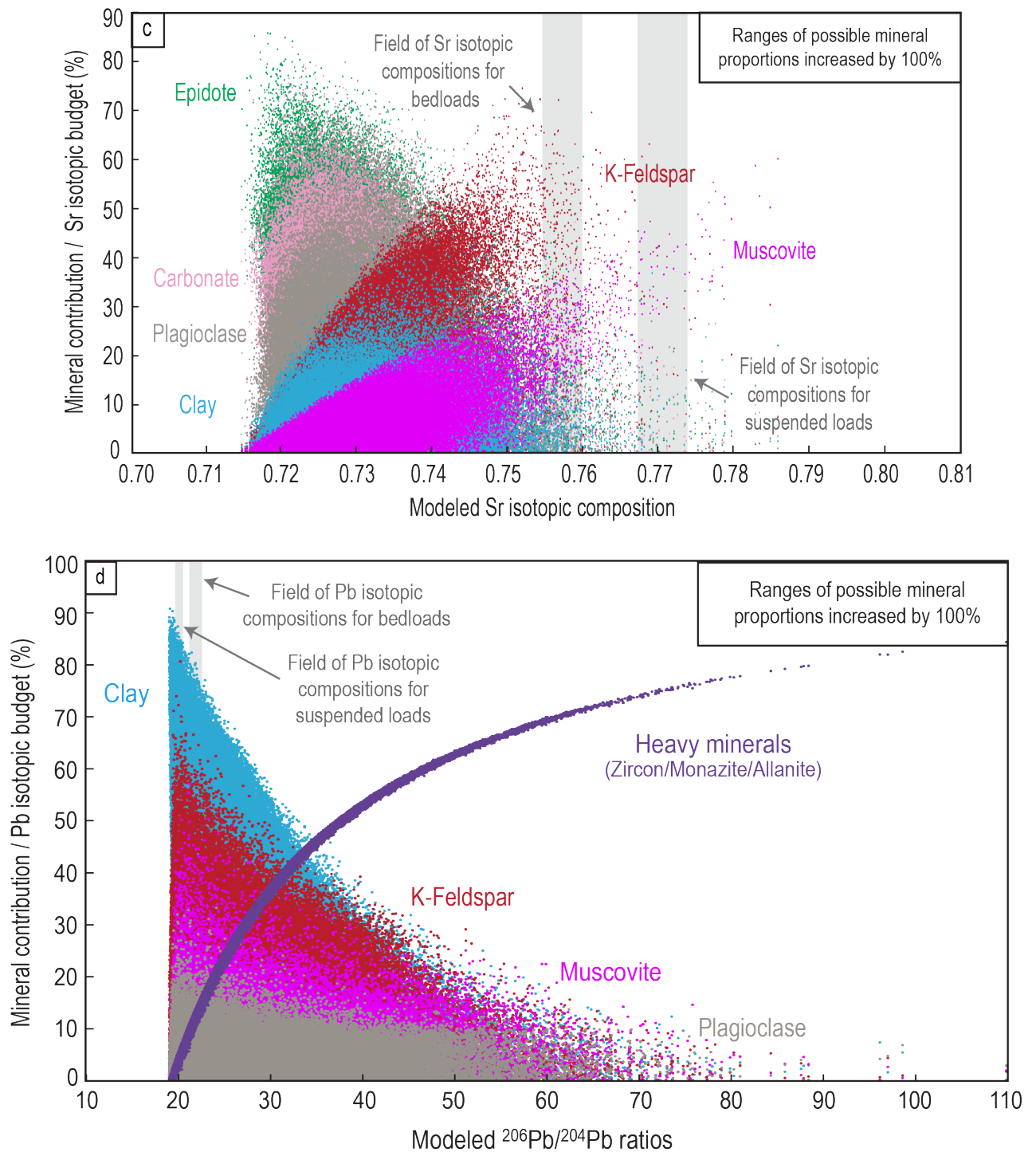


Figure A: Results of the Monte-Carlo simulations when increasing the input ranges of mineral proportions.

a) Nd; b) Hf; c) Sr and d) Pb. These simulations were performed using the same minerals as those considered in Figures 3, 5, 7 and 9 but using proportion ranges much larger (values provided in the second column of Table A). Minerals that contribute to less than 10% of the isotopic budgets are not

shown in the figures. Note that the ranges of modeled Sr isotopic compositions simulations still remain incompatible with the ranges measured for suspended loads from the Ganga River.

Supplementary Table 1: Weight mineral proportions in Ganga sediments modified after Garzanti et al. (2010, 2011)

Surface suspended loads (<3m)					Deep suspended loads (>8m)					Bedloads				
	Average	2 σ	Minimum	Maximum		Average	2 σ	Minimum	Maximum		Average	2 σ	Minimum	Maximum
Quartz	34.3	22.8	26.2	42.4	Quartz	48.7	10.6	43.2	54.1	Quartz	55.4	14.9	39.8	66.0
K-feldspar	2.6	1.6	2.1	3.2	K-feldspar	5.7	2.3	4.3	6.9	K-Feldspar	6.6	3.1	3.9	8.5
Albite	4.6	2.4	3.8	5.4	Albite	5.9	4.0	3.9	8.2	Plagioclase	6.0	2.9	2.9	7.4
Ca-plagioclase	2.4	2.3	1.6	3.2	Ca-plagioclase	4.2	2.8	3.5	6.4					
Lithic grain	ND				Lithic grain	ND				Lithic grain	14.5	5.2	10.9	18.6
Calcite	1.2	0.3	1.1	1.3	Calcite	2.9	1.6	1.9	3.7	Calcite*	3.4	2.5	0.5	4.7
Dolomite	1.8	0.2	1.7	1.9	Dolomite	2.3	2.1	1.1	3.5	Dolomite	ND			
Muscovite	17.5	9.2	14.2	20.7	Muscovite	8.9	5.4	5.0	11.0	Micas	9.8	21.9	2.2	36.1
Biotite	10.4	4.3	8.8	11.9	Biotite	5.5	3.0	3.8	7.3					
Chlorite	2.8	1.4	2.4	3.3	Chlorite	1.7	1.1	1.1	2.3	Chlorite	ND			
Clay	19.5	18.6	12.9	26.0	Clay	9.8	3.6	8.2	12.0	Clay	ND			
Fe-oxides	0.2	0.2	0.2	0.3	Fe-oxides	0.1	0.1	0.02	0.1	Fe-oxides	ND			
Fibrolite	ND				Fibrolite	ND				Fibrolite	0.1	0.2	0	0.3
Opagues	1.3	0.1	1.2	1.3	Opagues	1.0	0.7	0.8	1.6	Opagues	1.1	2.8	0.1	3.7
Zircon	0.1	0.02	0.1	0.1	Zircon	0.1	0.3	0.03	0.4	Zircon	0.1	0.4	0	0.5
Tourmaline	0.2	0.1	0.2	0.3	Tourmaline	0.2	0.1	0.2	0.3	Tourmaline	0.3	0.7	0.1	1.1
Rutile	0.2	0.2	0.1	0.3	Rutile	0.2	0.2	0.1	0.3	Rutile	0.1	0.2	0	0.2
Ti oxide	0.4	0.1	0.4	0.4	Ti oxide	0.2	0.2	0.1	0.3	Ti oxide	0.0	0.1	0	0.2
Titanite	0.1	0.1	0.1	0.2	Titanite	0.2	0.3	0.1	0.5	Titanite	0.3	0.5	0.05	0.7
Apatite	0.1	0.04	0.1	0.1	Apatite	0.1	0.1	0.03	0.1	Apatite	0.1	0.4	0	0.5
Monazite	ND				Monazite	ND				Monazite	0.1	0.3	0	0.4
Amphibole	0.5	0.6	0.3	0.7	Amphibole	1.1	0.6	0.9	1.6	Amphibole	1.4	2.0	0.4	3.0
Pyroxene	0.2	0.1	0.2	0.3	Pyroxene	0.3	0.2	0.2	0.4	Pyroxene	0.3	0.5	0.1	0.8
Spinel	ND				Spinel	ND				Cr-spinel	ND		0	0.0
Epidote	1.4	0.8	1.1	1.7	Epidote	1.0	0.3	0.8	1.1	Epidote	1.0	1.5	0.2	2.2
Allanite	ND				Allanite	0.02	0.1	0	0.1	Allanite	ND		0	0.0
Chloritoid	ND				Chloritoid	ND				Chloritoid	ND		0	0.1
Garnet	0.4	0.5	0.3	0.6	Garnet	1.2	1.9	0.5	2.6	Garnet	2.8	6.5	0.2	8.2
Staurolite	ND				Staurolite	0.03	0.02	0.02	0.04	Staurolite	0.1	0.1	0	0.2
Kyanite	0.04	0.1	0.0	0.1	Kyanite	0.1	0.1	0.07	0.19	Kyanite	0.2	0.5	0	0.7
Sillimanite	ND				Sillimanite	0.1	0.1	0.03	0.2	Sillimanite	0.02	0.1	0	0.1
<i>Sum</i>	102.2				<i>Sum</i>	101.4				<i>Sum</i>	103.7			

Minerals taken into account in our Monte-Carlo simulations are highlighted in gray.

ND: not determined or under detection limit

*not determined by Garzanti et al. (2010; 2011). Values from Lupker et al. (2012)

Supplementary Table 2: Trace element concentrations and Nd-Hf-Pb isotopes in sediments sampled at the outflow of the Ganga River from Garçon et al. (2013a; 2013b)

Sample Name	BGP 6	BGP 6 Dup	BR 415	BR 414	BR 413	BR 412	BR 411	BR 418	BR 8252	BR 8253	BR 717
Type of sediment	Bedload	Bedload	Suspended Load	Suspended Load	Suspended Load	Suspended Load	Suspended Load	Bedload	Bedload	Suspended Load	Bedload
Sampling depth (m)			0	2	4	6.5	9	10	14	0	11
Cs	3.83	4.02	15.4	13.6	11.8	11.7	8.08	2.64	3.05	8.92	3.87
Rb	77.9	85.2	202	186	174	175	107	56.6	34.5	51.7	50.3
Ba	294	307	627	562	531	527	372	212	203	240	244
Th	30.2	31.3	20.0	19.0	19.3	18.0	15.1	29.7	24.3	16.1	74.2
U	5.41	5.71	4.64	4.08	4.15	3.96	2.92	5.14	3.33	1.85	11.7
Nb	12.9	12.0	17.4	17.9	16.5	15.7	13.6	18.4	13.6	15.8	20.3
Ta	1.78	1.44	1.54	1.57	1.45	1.39	1.37	2.08	2.91	1.31	2.50
La	67.1	70.2	42.0	41.3	42.2	40.0	32.8	71.0	41.6	30.8	141
Ce	144	145	89.4	88.1	89.2	84.7	76.3	146	110	75.4	292
Pr	15.5	16.4	9.75	9.77	9.87	9.29	7.84	16.7	10.6	8.12	33.1
Pb	17.8	17.6	30.4	28.2	25.3	17.4	15.0	10.7	10.7	10.5	14.2
Nd	56.5	60.8	35.0	35.7	35.8	34.0	29.0	60.4	39.4	31.2	121
Sr	115	117	84.1	91.0	99.3	101	88.6	103	83.6	56.5	98.3
Sm	10.9	11.4	6.93	6.98	7.01	6.77	5.60	12.0	7.63	6.27	22.3
Zr	683	667	178	204	227	199	249	479	403	196	1550
Hf	17.1	17.4	4.73	5.22	5.79	5.17	6.14	12.1	10.5	5.13	40.5
Ti	3155	3166	4137	4198	3976	3833	3314	4355	2523	4323	5299
Eu	1.39	1.45	1.27	1.26	1.23	1.20	1.04	1.48	0.928	1.19	2.24
Gd	8.51	9.10	6.19	6.15	6.05	5.80	4.96	10.1	6.41	5.44	17.7
Tb	1.25	1.29	0.984	0.945	0.93	0.872	0.782	1.64	0.977	0.854	2.52
Dy	7.24	7.61	5.97	5.74	5.72	5.42	4.81	10.3	5.70	5.32	14.7
Ho	1.39	1.48	1.17	1.15	1.13	1.06	0.95	2.12	1.16	1.06	2.83
Y	41.1	43.5	32.7	32.8	32.5	30.9	27.1	62.0	34.5	31.1	85.6
Er	3.99	4.24	3.33	3.30	3.21	3.07	2.85	6.35	3.33	3.04	8.11
Li	14.7	16.3	51.8	48.2	43.5	41.9	32.2	15.8	12.6	45.3	15.7
Yb	3.87	4.16	3.18	3.11	3.06	2.88	2.51	6.23	3.32	2.95	8.17
Lu	0.587	0.614	0.461	0.45	0.448	0.417	0.366	0.905	0.50	0.433	1.25
Sc	7.74	9.81	15.0	14.4	13.5	12.8	9.04	13.2	4.56	11.8	14.3
V	32.7	34.8	93.4	90.7	81.1	79.1	61.8	46.9	34.5	100	53.5
Cr	36.9	38.4	76.6	81.9	67.0	63.4	53.4	40.0	28.2	73.6	44.1
Co	3.93	4.32	15.5	15.1	13.6	13.4	10.3	5.58	4.46	13.8	6.40
Ni	11.0	11.3	38.6	40.5	32.4	31.5	26.4	11.7	9.39	39.4	12.4
¹⁴³ Nd/ ¹⁴⁴ Nd ± 2σ	0.511758 ± 9	0.511749 ± 7	0.511752 ± 6	0.511736 ± 8	0.511748 ± 6	0.511745 ± 7	0.511755 ± 6	0.511719 ± 5	0.511788 ± 11	0.511767 ± 8	0.511769 ± 7
¹⁷⁶ Hf/ ¹⁷⁷ Hf ± 2σ	0.282027 ± 11	0.282009 ± 7	0.282241 ± 9	0.282226 ± 6	0.282205 ± 6	0.282209 ± 6	0.282133 ± 7	0.281992 ± 11		0.282268 ± 7	0.281930 ± 6
²⁰⁸ Pb/ ²⁰⁴ Pb ± 2σ	40.6213 ± 43	40.579 ± 39	40.3003 ± 18	40.3019 ± 25	40.2931 ± 34	40.2725 ± 16	40.1312 ± 28	40.8292 ± 23	40.8030 ± 26	39.9963 ± 28	42.4525 ± 27
²⁰⁷ Pb/ ²⁰⁴ Pb ± 2σ	15.9733 ± 14	15.9644 ± 13	15.8991 ± 6	15.9013 ± 5	15.904 ± 7	15.9040 ± 6	15.8984 ± 10	15.9684 ± 9	15.9548 ± 9	15.873 ± 13	16.1109 ± 9
²⁰⁶ Pb/ ²⁰⁴ Pb ± 2σ	20.7277 ± 14	20.6899 ± 18	20.0301 ± 7	20.0574 ± 9	20.0912 ± 8	20.0756 ± 7	20.0387 ± 11	20.6767 ± 9	20.5845 ± 10	19.7765 ± 10	22.1618 ± 10